

---

**Messung der Trigger Effizienzen im ATLAS  
Detektor für Suchen nach Supersymmetrie in  
Ereignissen mit Tauleptonen im Endzustand**

---

**Measurement of the trigger efficiencies in the  
ATLAS detector for searches for supersymmetry  
in events with tau leptons in the final state**

---



Masterarbeit an der Fakultät für Physik  
der Ludwig-Maximilians-Universität München

vorgelegt von

**Marina Steimle**

geboren in Landshut

München, den 11.05.2016

---

Gutachterin: Prof. Dr. Dorothee Schaile

# Abstract

The Large Hadron Collider (LHC) at CERN collides particles, either protons or heavy ions, at very high energies in the TeV range in order to test the Standard Model (SM) of particle physics and to search for new physics beyond the SM. One of the main purposes of the ATLAS detector, one of the major experiments at the LHC, is the search for supersymmetry, a theory which can solve most of the open questions of the Standard Model.

An interesting search channel is the electroweak production of supersymmetric particles, if strongly produced particles are too heavy to be created at the LHC. In this thesis a scenario where the decay of these particles leads to a final state containing at least two tau leptons is considered. To select such events a trigger demanding two hadronically decaying taus with high transverse momentum, called di-tau trigger, is used.

The objective of this thesis is to measure the efficiency of this trigger using the full data recorded in 2015 by the ATLAS detector in proton-proton collisions at a center-of-mass energy  $\sqrt{s} = 13$  TeV, corresponding to an integrated luminosity of  $3.2 \text{ fb}^{-1}$ .

The di-tau trigger is too complex to measure the efficiency directly in data, therefore it is done in two steps. Firstly the trigger is split into its two components, where each component corresponds to a single tau trigger. The single tau triggers select events which contain at least one hadronically decaying tau. For each single tau trigger the efficiency is determined separately in data with a ‘tag-and-probe’ method and the result is compared to Monte-Carlo simulations. Secondly it is proven with a closure test using MC simulations that the two components are independent from each other and that therefore the di-tau trigger efficiency can be calculated as the product of the efficiencies of the two single tau triggers.



# Zusammenfassung

Der ‘Large Hadron Collider (LHC) am CERN kollidiert Teilchen, entweder Protonen oder schwere Ionen, bei sehr hohen Energien in der Größenordnung von  $\sim 10$  TeV, um das Standard Modell (SM) der Teilchenphysik zu testen und um nach neuer Physik jenseits des SM zu suchen. Eine der Hauptaufgaben des ATLAS Detektors, eines der größten Experimente am LHC, ist die Suche nach Supersymmetrie, einer Theorie, die die meisten offenen Fragen des Standard Modells lösen kann.

Ein interessanter Suchkanal dafür ist die elektroschwache Produktion von supersymmetrischen Teilchen, falls die Teilchen, die durch die starke Wechselwirkung produziert werden, zu schwer sind, um am LHC erzeugt zu werden. In dieser Arbeit wird ein Szenario betrachtet, in dem der Zerfall dieser Teilchen zu einem Endzustand führt, der mindestens zwei Tauleptonen enthält. Um derartige Ereignisse auszuwählen, wird ein Trigger verwendet, der zwei hadronisch zerfallende Taus mit hohen transversalen Impuls fordert und der Di-Tau Trigger genannt wird.

Ziel dieser Arbeit ist es, die Effizienz dieses Triggers mithilfe des Datensatzes an Proton-Proton Kollisionen, der 2015 mit dem ATLAS Detektor bei einer Schwerpunktenergie von  $\sqrt{s} = 13$  TeV aufgenommen wurden, zu messen. Dieser entspricht einer integrierten Luminosität von  $3.2 \text{ fb}^{-1}$ .

Der Di-Tau Trigger ist zu komplex, um seine Effizienz direkt in den Daten zu messen, deswegen wird die Messung in zwei Schritte aufgeteilt. Im ersten Schritt wird der Trigger in seine zwei Komponenten gespalten, wobei jede Komponente einem ‘Single Tau Trigger’ entspricht. Die Single Tau Triggers selektieren Ereignisse, die mindestens ein hadronisch zerfallendes Tau beinhalten. Für jeden der zwei Single Tau Triggers wird die Effizienz in den Daten separat mit einer ‘Tag-and-Probe’ Methode bestimmt und das Ergebnis mit Monte-Carlo Simulationen verglichen. Im zweiten Schritt wird durch einen ‘Closure’ Test mit MC Simulationen bewiesen, dass die beiden Komponenten des Di-Tau Triggers unabhängig voneinander sind und dass deshalb seine Trigger Effizienz aus dem Produkt der zwei Single Tau Trigger Effizienzen berechnet werden kann.



# Contents

<b>1</b>	<b>Introduction</b>	<b>1</b>
<b>2</b>	<b>Theory</b>	<b>3</b>
2.1	The Standard Model . . . . .	3
2.2	Supersymmetry . . . . .	7
2.3	Electroweak Production of Supersymmetric Particles . . . . .	10
<b>3</b>	<b>Experiment</b>	<b>13</b>
3.1	The Large Hadron Collider . . . . .	13
3.2	The ATLAS Detector . . . . .	14
3.2.1	ATLAS Coordinate System . . . . .	15
3.2.2	Inner Detector . . . . .	15
3.2.3	Calorimeters . . . . .	16
3.2.4	Muon Spectrometer . . . . .	16
3.2.5	Particle Identification . . . . .	16
3.2.6	Trigger System . . . . .	18
<b>4</b>	<b>Data and Monte Carlo Samples</b>	<b>21</b>
4.1	Data Samples . . . . .	21
4.2	Monte Carlo Samples . . . . .	21
4.2.1	Standard Model Background Samples . . . . .	22
4.2.2	SUSY Signal Samples . . . . .	22
<b>5</b>	<b>Object and Event Selection</b>	<b>23</b>
5.1	Object selection . . . . .	23
5.2	Overlap Removal . . . . .	26
5.3	Basic Event Selection . . . . .	26
<b>6</b>	<b>General Strategy for Measurement of Trigger Efficiencies</b>	<b>29</b>
6.1	Trigger Nomenclature . . . . .	29
6.2	Trigger Efficiency: Turn-on Curves . . . . .	31
6.3	Single Tau Trigger Efficiency in Data: Tag-and-Probe Method . . . . .	32
6.4	Di-Tau Trigger Efficiency: Factorization and Closure Test . . . . .	34

---

<b>7</b>	<b>Background Estimation</b>	<b>35</b>
7.1	Trigger Scale Factors for Light Lepton Triggers . . . . .	36
7.2	Multi-Jet and General Background Estimation . . . . .	36
7.3	Preselection . . . . .	38
7.3.1	Tau-Muon Selection . . . . .	38
7.3.2	Tau-Electron Selection . . . . .	39
7.4	W Control Region: Scale Factors $k_W^{\text{OS}}$ and $k_W^{\text{SS}}$ . . . . .	39
7.5	QCD control region . . . . .	44
7.6	W Control Region: Background Estimation . . . . .	47
7.7	Z Control Region . . . . .	49
<b>8</b>	<b>Results: Efficiency of the Di-Tau Trigger</b>	<b>55</b>
8.1	Efficiency of Single Tau Triggers . . . . .	55
8.2	Efficiency of the Di-Tau Trigger . . . . .	58
<b>9</b>	<b>Conclusion</b>	<b>61</b>
<b>A</b>	<b>MC Background and Signal Samples</b>	<b>63</b>
<b>B</b>	<b>Additional Plots</b>	<b>65</b>
	<b>Danksagung</b>	<b>75</b>



# Chapter 1

## Introduction

In the last century the Standard Model (SM) of particle physics, a theory which describes the interactions between the elementary particles and three of the four fundamental forces, was developed. With the discovery of a new particle in 2012, consistent with the expectations of the Higgs boson, the last piece of the SM was found. The existence of the Higgs boson is predicted by the Higgs mechanism, a theory which explains how the  $W$  bosons, the  $Z$  boson and the fermions acquire their mass. The SM was (and still is) investigated in many experiments in the last decades and to a very high precision an agreement between experiments and theory was found. It is considered a well-tested theory of the visible matter in the universe.

However despite the success, there are several open questions which can not be solved within the SM. This indicates that there must be new physics beyond the SM. There are many ideas and theories of what this physics could be, but so far no experimental evidence from particle colliders was found to support any of these theories.

To search for new physics and to test the SM particles in colliders, for example protons, are accelerated in two beams to very high energies before they collide. The results of the collisions are then recorded and can be studied. The largest and most powerful particle collider at the moment is the Large Hadron Collider (LHC) at CERN, which collides proton beams with a center-of-mass energy  $\sqrt{s} = 13 \text{ TeV}$ . One of the main experiments at the LHC is the ATLAS detector, a multi-purpose detector, which among other things searches for evidence of Supersymmetry (SUSY).

Supersymmetry is a theoretical concept which would solve most of the problems of the SM. The main idea of SUSY is that every particle in the SM has a super-partner with a spin differing by  $1/2$  with respect to the SM particle. There are many ways in which this concept can be used to predict new particles and how they are produced with proton-proton collisions and detected in the ATLAS detector. The produced new particles cannot be directly observed, since they decay into other particles, which either can be detected or leave the detector without interaction, (if they are neutral and don't interact strongly) leading to large missing energy in an event. Looking at a specific final state recorded in the detector and studying this state in detail conclusions about the produced particles can be drawn.

The final state considered in this thesis consists of two hadronically decaying tau-leptons and missing transverse energy, where it is assumed that potential supersymmetric particles are produced in pairs and via the electroweak force. It is also assumed that these particles decay through the super-partner of the tau lepton, therefore leading to final states with taus.

The rate of proton-proton collisions in the LHC is about 600 millions per second. This is far too much to save every single collision, therefore triggers are used to pick interesting events which will be recorded. In this thesis a trigger, selecting events with two hadronically decaying tau-leptons, is studied and its efficiency is measured using the data recorded with the ATLAS detector in 2015.

The thesis is organized in the following way. In Chapter 2 an overview of the theoretical background is given. It is divided into three parts, the first one is about the SM and its open questions. The second part consists of a short introduction of supersymmetry while in the last part the electroweak production processes of the supersymmetric particles used in this thesis are explained. In Chapter 3 the experimental setup of the LHC and the ATLAS detector are described. The data and Monte Carlo (MC) samples used in the thesis are given in Chapter 4. Chapter 5 explains the selection criteria of the different physical objects used and the basic event selection. The general strategy for the measurement of trigger efficiencies is explained in Chapter 6 where more information about the triggers used in the thesis, and how the determination of the trigger efficiencies vary between data and MC simulation, are given. The background estimation, used for the trigger efficiency measurement in data, is shown in Chapter 7. In Chapter 8 the results of the measurements are given while finally in the last Chapter 9 all results are summarized.

# Chapter 2

## Theory

In the following a brief overview of the theoretical foundations needed for this thesis is given. After a short introduction to the Standard Model of particle physics and its open issues, the motivation and concepts of Supersymmetry are described and in the final part the processes considered for this thesis are presented.

### 2.1 The Standard Model

The Standard Model (SM) of particle physics is a successful theoretical framework which describes the fundamental particles and their interactions. It was developed in the 20th century and its theoretical predictions were confirmed in many experiments. In this section a short overview of the SM is given based on [1], [2] and [3].

The particle content of the SM can be divided in two different groups based on the particle spin: the fermions with spin  $1/2$  and the bosons with integer spin. The fermions can be further classified in subgroups as quarks and leptons. Each subgroup consists of three generations where the second and third generations are more massive ‘copies’ of the first one, i.e. they have similar properties but higher masses. Each generation consists of an up- and down-like quark and a charged lepton and a neutral lepton, the neutrino. In Table 2.1 the fermions of the SM are summarized and their respective charges and masses are given. For every fermion there also exists an antiparticle, a particle with the exact same mass and spin, but with opposite signs in the charge quantum numbers.

The bosons can be separated into the gauge bosons with spin 1, which mediate the forces between the particles, and the Higgs boson with spin 0, whose existence is predicted by the Higgs mechanism. Three of the four fundamental forces are described within the SM, the strong, the electromagnetic and the weak force. The fourth one, gravity, is not included into the SM. The strong force is mediated by eight massless gluons, which differ by their color charge, and it is responsible for the quarks to be bound in hadronic states and also to keep protons and neutrons together in the nuclei. The gluons can only couple to colored particles, i.e. either quarks or other gluons. The electromagnetic force is mediated by the massless photon and it couples to the electric charge of particles. There are three massive

### Quarks

generation	name	symbol	charge [e]	mass [MeV]
1	up	$u$	$2/3$	2.3
	down	$d$	$-1/3$	4.8
2	charm	$c$	$2/3$	$1.275 \cdot 10^3$
	strange	$s$	$-1/3$	95
3	top	$t$	$2/3$	$173.2 \cdot 10^3$
	bottom	$b$	$-1/3$	$4.18 \cdot 10^3$

### Leptons

generation	name	symbol	charge [e]	mass [MeV]
1	electron	$e$	$-1$	0.511
	electron-neutrino	$\nu_e$	0	$< 2 \cdot 10^{-6}$
2	muon	$\mu$	$-1$	105.7
	muon-neutrino	$\nu_\mu$	0	$< 0.19$
3	tau	$\tau$	$-1$	1776.9
	tau-neutrino	$\nu_\tau$	0	$< 18.2$

Table 2.1: The fermions of the SM [4].

mediators of the weak force, two charged  $W^\pm$  bosons and one neutral  $Z$  boson which couple to the weak isospin. The bosons and their most important properties are summarized in Table 2.2.

interaction	name	symbol	spin	charge [e]	mass [GeV]
strong	gluon	$g$	1	0	0
electromagnetic	photon	$\gamma$	1	0	0
weak	$W$ boson	$W^\pm$	1	$\pm 1$	80.385
	$Z$ boson	$Z$	1	0	91.1876
-	Higgs boson	$H^0$	0	0	125.09

Table 2.2: The bosons of the SM [4].

The mathematical framework used to describe the particles and their interaction is called Quantum Field Theory (QFT), which combines the aspects of special relativity and quantum mechanics.

Similarly to the Lagrange function  $L(q_i, \dot{q}_i, t)$  (depending on the coordinates  $q_i$ , their time derivatives  $\dot{q}_i$  and the time  $t$ ) in classical mechanics, in QFT a Lagrangian (density)  $\mathcal{L}(\Phi, \partial_\mu \Phi, x^\mu)$  with the field  $\Phi(\vec{x}, t)$ , the space-time derivative of the field  $\partial_\mu \Phi = \partial \Phi / \partial x^\mu$

and the space-time coordinates  $x^\mu = (ct, x, y, z)$  is defined. With the principle of least action the Euler-Lagrange equation in field theory can be derived:

$$\partial_\mu \left( \frac{\partial \mathcal{L}}{\partial (\partial_\mu \Phi)} \right) = \frac{\partial \mathcal{L}}{\partial \Phi}$$

which results in the equation of motion for the field. If more than one field is part of the Lagrangian, there is one such equation for every field. The SM is described by a quantum field theory with three gauge symmetries. A gauge symmetry means that the Lagrangian must be invariant under a continuous group of local transformation, i.e. changing the field  $\Phi \rightarrow \Phi' = e^{i\theta(x^\mu)}\Phi$  does not change the Lagrangian. The fundamental gauge symmetries of the SM are the combination of three symmetry groups:  $SU(3)_C \otimes SU(2)_L \otimes U(1)_Y$ .

$SU(3)_C$  describes the strong interaction of particles carrying color (C) charge and is called quantum chromodynamics (QCD). The weak interaction can not be treated in a gauge theory of its own. It is unified with the electromagnetic interaction to the electroweak interaction which is represented by  $SU(2)_L \otimes U(1)_Y$  and was developed by Glashow, Weinberg and Salam (GWS theory). For that a new charge, the hypercharge  $Y$  was constructed, which is related to the electric charge  $Q$  and the third component of the weak isospin  $I_3$  by:

$$Y = 2(Q - I_3).$$

The subscript L stands for the fact that only left-handed fermions participate in the weak interaction. The electroweak interaction demands massless gauge bosons, because introducing mass terms in the theory would break the local gauge invariance. However in experiment it was found that the  $W$  and  $Z$  bosons are massive. To solve this problem the Higgs mechanism was proposed. For that a complex scalar field, called Higgs field, was introduced with a non zero vacuum expectation value, and the  $SU(2)_L \otimes U(1)_Y$  symmetry is spontaneously broken. After the symmetry breaking the  $W$  and  $Z$  boson acquire their masses. Additionally another scalar particle, the Higgs boson, must exist. The fermions get their mass by coupling to the Higgs field via the Yukawa interaction.

## Open Issues of the Standard Model

The SM describes the elementary particles, their properties and the interaction between them and predicts experimental observations to high precision. Nevertheless there are a number of open questions which can not be explained within the Standard Model.

### Gravity

As already mentioned the gravitational force is not included in the SM. Gravity is the weakest force and is in general neglected in particle physics. The energy scale, at which gravity would become important, is the Planck scale at  $10^{19}$  GeV and therefore far above the energy scale of the current experiments ( $\sim 10^4$  GeV).

## Dark matter and dark energy

Due to astronomical and cosmological observations it is known that only about 5% of the energy density in the universe is visible matter, i.e. the matter described by the SM, while about 27% consists of dark matter, some new form of matter not explained by the SM, observed due to its gravitational interaction. The rest, about 68% is called dark energy which is responsible for the accelerated expansion of the universe.

## Unification of forces

The successful unification of the electromagnetic and weak force motivated to try to also include the strong force, in a so-called Grand Unified Theory (GUT). In a GUT theory all three forces would be a different manifestation of a single interaction associated with one gauge group. Since the coupling constants of the different forces are not constant but depend on the energy it is possible to extrapolate them to high energies of about  $10^{16}$  GeV where they should reach the same value. This is not the case for the SM, the coupling constants do cross but not at one point (see Figure 2.1).

### Unification of the Coupling Constants in the SM and the minimal MSSM

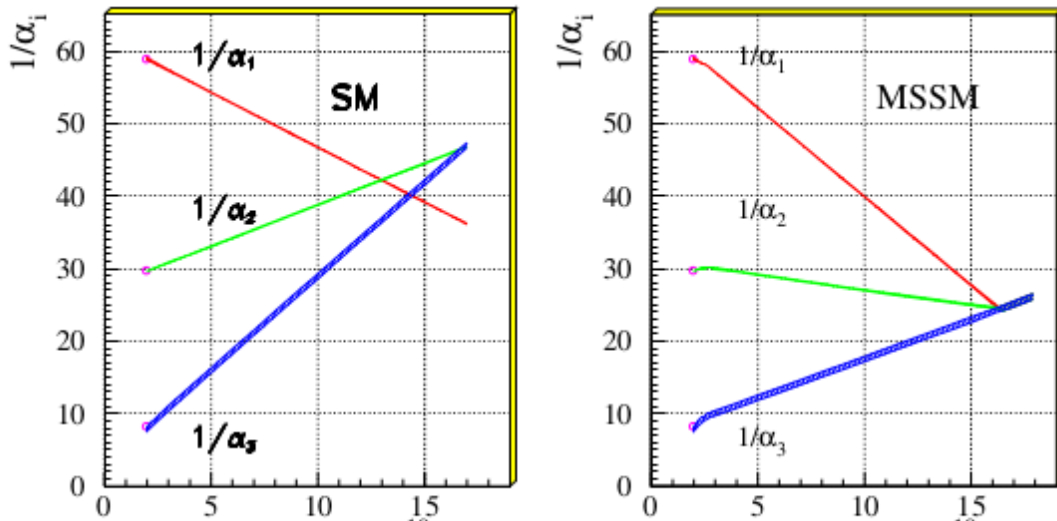


Figure 2.1: Evolution of the three inverse coupling constants in the SM (left) and in a supersymmetric extension (right). The coupling constants  $\alpha_1$ ,  $\alpha_2$  and  $\alpha_3$  correspond to the U(1), SU(2) and SU(3) coupling constants [5].

### Fine-tuning of the Higgs mass

Due to theoretical reasons the mass of the Higgs boson should not be too different from the mass of the  $W$  and  $Z$  boson, which was confirmed with the discovery of the Higgs boson at a mass of about 125 GeV. However the Higgs mass is very sensitive to quantum corrections from particles coupling to the Higgs field due to loop diagrams. For example the correction from a fermionic loop diagram is given according to [6] by:

$$\Delta m_H^2 = -\frac{|\lambda_f|^2}{8\pi^2} \Lambda_{\text{UV}}^2 + \dots$$

$\lambda_f$  is the coupling strength of the fermion and  $\Lambda_{\text{UV}}$  the ultraviolet momentum cutoff, which should be at least of the order of the energy scale at which the high energy behavior of the theory is changed by new physics. If there is no new physics before the energy scale would be the Planck scale ( $\sim 10^{19}$  GeV). Therefore the quantum correction to the Higgs mass would be many order of magnitude higher than the actual Higgs mass. So to achieve such a low Higgs mass, a high amount of fine-tuning would be needed in the SM for the quantum correction to cancel each other.

## 2.2 Supersymmetry

Supersymmetry (SUSY) is a promising extension of the Standard Model which can solve most of its open issues. In this section a short introduction to SUSY is given based on [6].

The main idea of supersymmetry is to introduce a symmetry transformation which turns a bosonic state into a fermionic state and vice versa with an operator  $Q$  generating this transformation:

$$Q|\text{Boson}\rangle = |\text{Fermion}\rangle, \quad Q|\text{Fermion}\rangle = |\text{Boson}\rangle.$$

Every particle in the SM gains a super-partner with a differing spin of 1/2 and with all other quantum numbers the same.  $Q^\dagger$ , the hermitian conjugate of  $Q$ , is also a generator of the supersymmetric transformation. Both carry spin 1/2 and are therefore fermionic operators and must fulfill the following anti-commutation and commutation relations:

$$\begin{aligned} \{Q, Q^\dagger\} &\propto P^\mu, \\ \{Q, Q\} &= \{Q^\dagger, Q^\dagger\} = 0, \\ [P^\mu, Q] &= [P^\mu, Q^\dagger] = 0, \end{aligned}$$

where  $P^\mu$  is the four-momentum generator of space-time translations. Since the squared mass operator  $-P^2$  also commutes with the operators  $Q$  and  $Q^\dagger$  it follows that the super-partners should have the same eigenvalues of  $-P^2$  and therefore the same mass as the SM particles. If that would be the case it would solve the fine-tuning problem of the Higgs mass, for every fermionic loop there is now a bosonic loop (and vice versa) which adds to the quantum corrections. Since there is a relative minus sign between fermionic and bosonic loop contributions they would cancel.

## Particle content of SUSY

Supersymmetric particles in general are called sparticles. The super-partners of the quarks and leptons are particles with spin zero. Their names are constructed by putting a ‘s’, for scalar, in front of the SM names. The symbols used for supersymmetric particles are the same as for the corresponding SM particles with a tilde above them. Since the left-handed and right-handed fermions transform differently under the gauge symmetries of the SM, each of them has its own scalar super-partner. For example, the super-partners of the left- and right-handed electron are called left- and right-handed selectrons and their symbols are  $\tilde{e}_L$  and  $\tilde{e}_R$ . Important to note is that the subscript ‘L’ and ‘R’ of the sfermions do not refer to their helicity but to that of their SM counterparts. Similarly the smuons and staus are denoted by  $\tilde{\mu}_L, \tilde{\mu}_R, \tilde{\tau}_L$  and  $\tilde{\tau}_R$ . Since the SM neutrinos (neglecting their very small masses) are always left-handed, the sneutrinos are denoted by  $\tilde{\nu}_e, \tilde{\nu}_\mu$  and  $\tilde{\nu}_\tau$ . The squarks, the super-partners of the quarks, are named analogously.

The super-partners of the gauge bosons have spin 1/2. They are named by adding ‘-ino’ at the end of the SM particle names, therefore they are generically referred to as gauginos. There are eight gluinos,  $\tilde{g}$  which are the super-partners of the gluons. For the electroweak gauge bosons the SUSY particles are called winos ( $\tilde{W}^\pm$ ), zino ( $\tilde{Z}$ ) and photino ( $\tilde{\gamma}$ ).

The super-partner of the Higgs boson is analogously called higgsino and has spin 1/2. For consistency reasons at least two complex Higgs doublets are needed. This leads to five physical Higgs bosons, two charged ( $H^\pm$ ) and three neutral ones ( $H^0, h^0, A^0$ ), instead of only the one Higgs boson needed in the SM. Since every Higgs boson should also have a super-partner, there are five higgsinos.

Because of the electroweak symmetry breaking the higgsinos and the electroweak gauginos mix with each other. The charged higgsinos ( $\tilde{H}^\pm$ ) and winos ( $\tilde{W}^\pm$ ) combine to form two mass eigenstates with charge  $\pm 1$  called charginos,  $\tilde{\chi}_i^\pm$  ( $i = 1, 2$ ) and the linear superposition of the neutral higgsinos ( $\tilde{H}^0, \tilde{h}^0, \tilde{A}^0$ ), the zino ( $\tilde{Z}$ ) and the photino ( $\tilde{\gamma}$ ) form four neutral mass eigenstates called neutralinos,  $\tilde{\chi}_i^0$  ( $i = 1, 2, 3, 4$ ). By convention the charginos and neutralinos are labeled according to the increasing mass of the particles, e.g. the  $\tilde{\chi}_1^0$  is therefore the lightest neutralino. Table 2.3 shows the particle content of the Minimal Supersymmetric Standard Model (MSSM), a supersymmetric extension of the SM with minimal particle content.

If gravity is included in the SUSY model the graviton, the theoretical spin-2 boson mediating gravity (it has not yet been discovered), has a super-partner with spin 3/2 called gravitino.

## Supersymmetry breaking

As already mentioned before the SUSY particles should have the same mass as their corresponding SM particles. If this were the case the lightest supersymmetric particles should have been already observed in experiments, for example there would have to be selectrons with mass equal to  $m_e = 0.511$  MeV. Since this is not the case, Supersymmetry must be a broken symmetry, where the supersymmetric particles can acquire a higher mass due to the



particle	symbol	spin	super-partner	symbol	spin
quarks, $q = u, d, c, s, t, b$	$q_L$	1/2	squarks	$\tilde{q}_L$	0
	$q_R$	1/2		$\tilde{q}_R$	0
leptons, $\ell = e, \mu, \tau$	$\ell_L$	1/2	sleptons	$\tilde{\ell}_L$	0
	$\ell_R$	1/2		$\tilde{\ell}_R$	0
	$\nu_\ell$	1/2		$\tilde{\nu}_\ell$	0
gluon	$g$	1	gluino	$\tilde{g}$	1/2
$W$ boson	$W^\pm$	1	charginos	$\tilde{\chi}_{1,2}^\pm$	1/2
charged Higgs boson	$H^\pm$	0			
$Z$ boson	$Z$	1	neutralinos	$\tilde{\chi}_{1-4}^0$	1/2
photon	$\gamma$	1			
neutral Higgs boson	$H^0, h^0, A^0$	0			

Table 2.3: The particle content of the MSSM.

symmetry breaking. For SUSY to still solve the fine-tuning problem this breaking should be ‘soft’, i.e. it should not change the masses too much (they should not be higher than the TeV scale), which is the energy scale accessible at the LHC. Another consequence is that the mass hierarchy of the SM particles need not be the same as for the SUSY particles, for example there are SUSY models where the stop is the lightest squark instead of the heaviest.

### ***R*-parity**

Supersymmetry in its most general form allows baryon ( $B$ ) and lepton number ( $L$ ) violation<sup>1</sup>, which can lead to the prediction of the proton decay (from experiments it is known that the lifetime of the proton is greater than  $10^{33}$  years). To ensure the proton stability in supersymmetric models often a new symmetry is introduced which forbids  $B$  and  $L$  violation. This symmetry is called ‘ $R$ -parity’ or ‘matter parity’ and is characterized by a multiplicative quantum number:

$$P_R := (-1)^{3(B-L)+2S}$$

where  $S$  is the spin of the particle. Due to the spin factor all SM particles have a  $R$ -parity of  $+1$ , while their super-partners have  $-1$ . If  $R$ -parity is conserved, there can be no mixing between particles and sparticles. This has some interesting phenomenological consequences:

<sup>1</sup>The baryon number of a system is defined as  $B = 1/3 \cdot (n_q - n_{\bar{q}})$  with  $n_q/n_{\bar{q}}$  the number of quark/anti-quarks in this system. The lepton number is similarly defined as  $L = n_\ell - n_{\bar{\ell}}$  where  $n_\ell/n_{\bar{\ell}}$  is the number of leptons/anti-leptons (charged leptons and neutrinos).

- The lightest supersymmetric particle (LSP) must be stable.
- Every other sparticle will eventually decay into the LSP.
- SUSY particles can only be produced in pairs.

### Solving the issues of the Standard Model

SUSY can provide solutions for most of the open issues of the SM and is therefore a promising theory for physics beyond the SM. As already mentioned before, gravity can be included into SUSY models by introducing the spin-3/2 super-partner of the graviton, the assumed mediator of gravity.

If  $R$ -parity is conserved and the lightest supersymmetric particle is electrically neutral, it only interacts via the weak force and is therefore a good candidate for dark matter.

The unification of the forces is not possible in the SM, the coupling constants do not converge into one point. In SUSY models however such a unification can be obtained if the SUSY particles have a mass around 1 TeV. The SUSY particles contribute to the running of the coupling constants and a merging of them at high energies is possible (see Figure 2.1).

The problem of fine-tuning can be solved, as already mentioned, due to the destructively interfering loop diagrams between the SM particles and their super-partners. The quantum corrections on the Higgs mass are of the same order for the particles and their corresponding sparticles, but they enter with a relative minus sign between them due to their different spin. This is only possible if the masses of the SUSY particles are not too high, compared to the SM particles.

## 2.3 Electroweak Production of Supersymmetric Particles

A wide variety of models are possible within SUSY, but for an analysis only a subset of models can be considered. For this thesis it is assumed that the supersymmetric particles, the charginos and neutralinos, are produced via the electroweak force and that the supersymmetric partner of the left-handed tau, the left-handed stau ( $\tilde{\tau}_L$ ), and the corresponding tau sneutrino ( $\tilde{\nu}_\tau$ ) are the only light sleptons. It is further assumed that these sparticles are light enough to be produced at the LHC and that the strongly interacting sparticles, the gluinos and squarks, are too heavy to be observed.

For SUSY to solve the fine-tuning problem, i.e. to protect the Higgs mass from quantum corrections, naturalness arguments suggest, that the masses of the charginos, of the neutralinos and of the lightest third generation sparticles should not be higher than a few hundred GeV. Additionally light sleptons in such a mass range, contributing to the co-annihilation of neutralinos in the early universe, are consistent with the cosmological observation of the dark matter relic density ([7] and [8]).

The dominant production process in such a model would be the  $\tilde{\chi}_1^\pm \tilde{\chi}_1^\mp$  and the  $\tilde{\chi}_1^\pm \tilde{\chi}_2^0$  process. If the two light sleptons ( $\tilde{\tau}_L$  and  $\tilde{\nu}_\tau$ ) are lighter than the  $\tilde{\chi}_1^\pm$  and  $\tilde{\chi}_2^0$  the possible decay processes are the following:  $\tilde{\chi}_1^\pm \rightarrow \tilde{\tau}_L \nu_\tau (\tilde{\nu}_\tau \tau) \rightarrow \tau \nu_\tau \tilde{\chi}_1^0$  and  $\tilde{\chi}_2^0 \rightarrow \tilde{\tau}_L \tau \rightarrow \tau \tau \tilde{\chi}_1^\pm$ . In so-called simplified models [9, 10] it is assumed that the charginos and neutralinos decay with a 100% branching fraction into the above defined final states. The diagrams associated with the production processes are shown in Figure 2.2. It is also possible that a stau pair is directly produced, where each stau would decay into a tau and the lightest neutralino. But this production process has a much smaller cross-section and is not considered in this thesis.

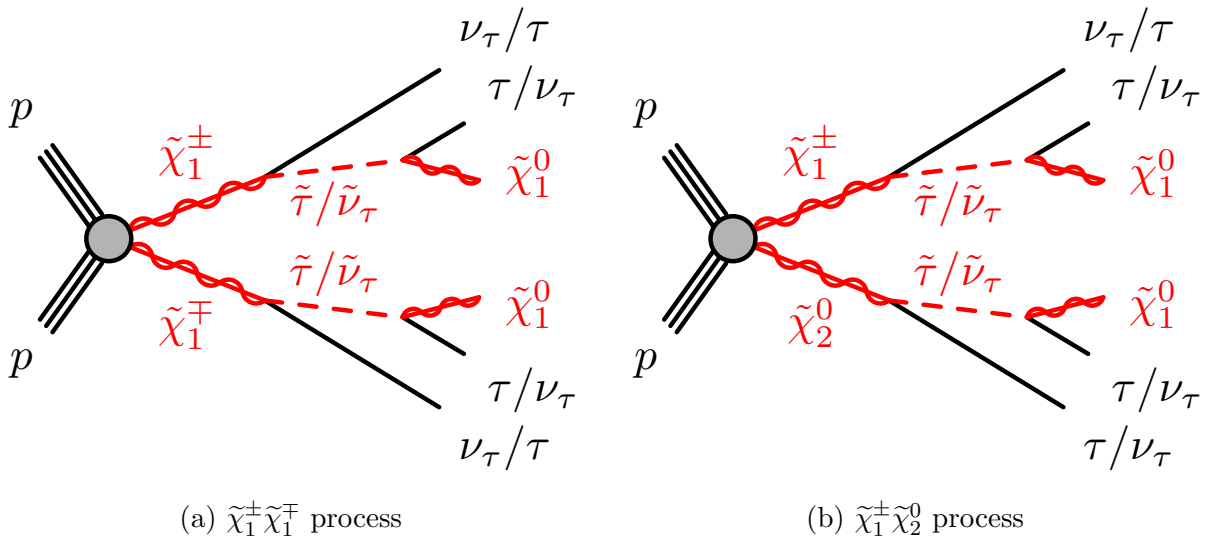


Figure 2.2: Diagrams of the considered electroweak production processes.

Therefore such events contain at least two taus and large missing transverse energy, due to the escaping neutrinos and neutralinos, in the final state. Only events in which the taus decay hadronically are considered. To select such events a trigger searching for two hadronically decaying tau with high transverse momentum is used. The objective of this thesis is to study this trigger in detail and to measure its efficiency.

Such a trigger can also be used by other analyses looking for strongly produced SUSY particles with final states containing taus. Such analyses would be for example [11] and [12].



# Chapter 3

## Experiment

### 3.1 The Large Hadron Collider

The Large Hadron Collider (LHC) at the European Organization for Nuclear Research (CERN) is at the moment the world largest and most powerful particle collider. CERN was founded in 1954 and is one of the most important institutions for high energy physics worldwide. It is located close to Geneva at the border between Switzerland and France and has 21 member states.

The LHC has a circumference of about 27 km and is designed to collide particle beams, consisting of either protons or lead-ions, at very high energies. In 2010 the LHC started operation with proton-proton collisions at a center-of-mass energy  $\sqrt{s} = 7$  TeV, which was increased to  $\sqrt{s} = 8$  TeV in 2012. In 2013, after the first run, the LHC shut down for two years of maintenance and repairs before it started operating again in 2015 with nearly twice the center-of-mass energy  $\sqrt{s} = 13$  TeV.

To accelerate the particles in the TeV range different pre-accelerators with increasingly higher energies are used before the particle beams are injected into the LHC (see Figure 3.1). For proton-proton (pp) collisions ionized hydrogen atoms are used. Starting with the linear accelerator LINAC2 the proton beam is injected into the PS Booster, where it reaches an energy of 1.4 GeV. After that the protons are sent to the Proton Synchrotron (PS) and then to the Super Proton Synchrotron (SPS), where they are accelerated to 25 GeV and 450 GeV respectively. They are then transferred to the LHC and split in clockwise and anti-clockwise beams. Each beam consists of 2808 bunches and each bunch contains about  $10^{11}$  protons. The beams are forced on a circular path and focused using magnetic fields up to 8.33 T [14].

There are four interaction points along the accelerator ring where the beams can collide, corresponding to the location of the four major particle detectors, ATLAS, CMS, LHCb and ALICE. ATLAS and CMS are both general-purpose detectors designed to cover a wide range of physics, from high precision tests of the Standard Model to beyond the Standard Model physics like e.g. Supersymmetry. One important objective of both detectors was the search for the Higgs boson which was found by both in 2012. LHCb specializes in

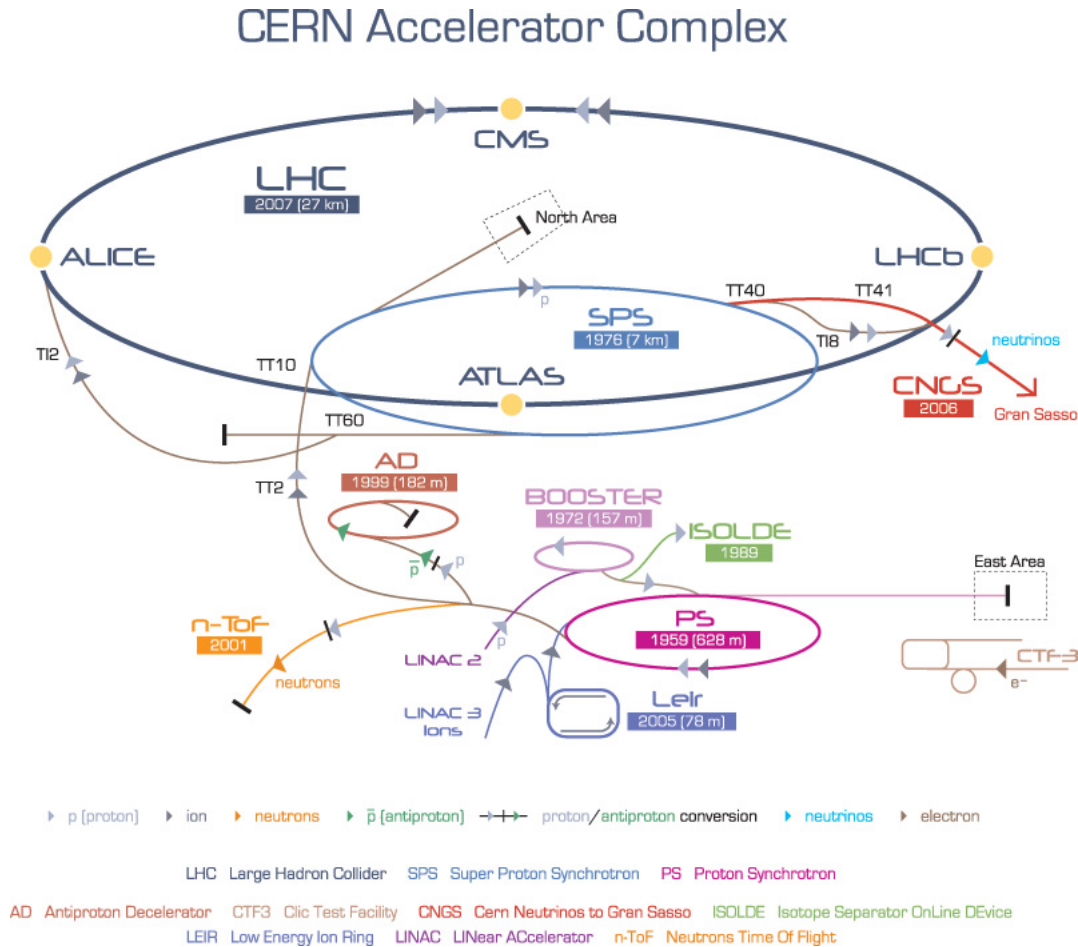


Figure 3.1: Schematic overview of the LHC and the smaller accelerators at CERN [13].

$B$ -physics (i.e. particles containing a  $b$ -quark) and studies the asymmetry between matter and antimatter. Finally ALICE is a heavy ion detector and is designed to study the physics of strongly interacting matter at high energy densities [15].

## 3.2 The ATLAS Detector

The ATLAS detector [16, 17] has a forward-backward cylindrical symmetry with respect to the interaction point and covers almost the full solid angle around the beam axis. The detector has four sub-detectors layered around the interaction point, starting with the inner detector (ID), followed by the electromagnetic and hadronic calorimeters and the muon chambers (see Figure 3.2). A combination of the informations from each sub-detector is used to identify the different particles and to measure their kinematics.

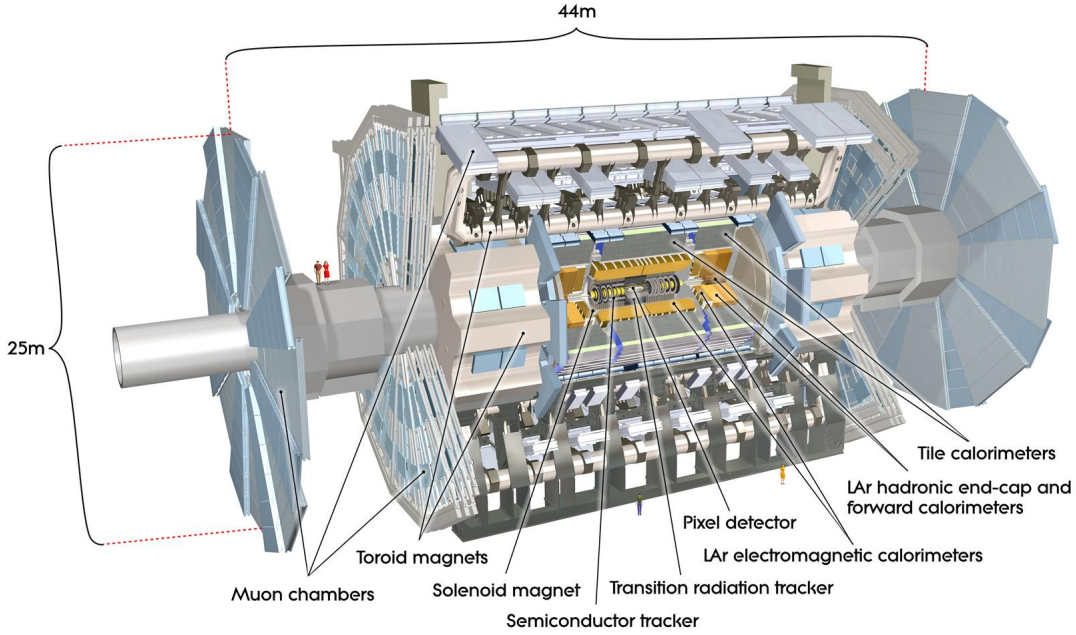


Figure 3.2: An overview of the ATLAS detector [18].

### 3.2.1 ATLAS Coordinate System

ATLAS uses a right-handed Cartesian coordinate system with its origin at the nominal interaction point (i.e. the center of the detector). The  $z$ -axis is defined along the beam axis and the  $x$ - $y$  plane perpendicular to the beam direction with the  $x$ -axis pointing to the center of the LHC and the  $y$ -axis pointing upwards. The azimuthal angle  $\phi$  is the angle around the  $z$ -axis and the polar angle  $\theta$  is measured with respect to the beam axis.

Instead of  $\theta$  often the pseudorapidity  $\eta = -\ln(\tan(\theta/2))$  or in cases with massive objects (e.g. jets) the rapidity  $\bar{y} = 1/2 \cdot \ln((E + p_z)(E - p_z))$  is used, where  $E$  is the energy and  $p_z$  is the component of the momentum along the beam axis. Distances in the  $\eta$ - $\phi$  space are defined as  $\Delta R = \sqrt{\Delta\eta^2 + \Delta\phi^2}$  and in the  $\bar{y}$ - $\phi$  space as  $\Delta\bar{R} = \sqrt{\Delta\bar{y}^2 + \Delta\phi^2}$ . The transverse variables, e.g. the transverse momentum  $p_T = \sqrt{p_x^2 + p_y^2}$  or the missing transverse energy  $E_T^{\text{miss}}$  are measured in the  $x$ - $y$  plane.

### 3.2.2 Inner Detector

The innermost layer of the ATLAS detector (ID) is a tracking detector and it is used to reconstruct the tracks of charged particles. It covers the whole  $\phi$ -range and the pseudorapidity range  $|\eta| < 2.5$ . It needs to provide precise momentum measurement and a good vertex resolution, while at the same time handling the large amount of tracks created by the collisions. The inner detector is immersed in a 2 T axial magnetic field provided by a solenoid and consists of three different tracking systems. Semiconductor pixel and sil-

icon microstrip detectors in the inner part of the detector are used for high vertex and momentum resolution. The outer part consists of straw-tube tracking detectors with the capability to generate and detect transition radiation, therefore called transition radiation tracker (TRT). The TRT contributes to the momentum measurement with lower precision but this is compensated by a higher number of measurement points. Additionally the TRT improves the electron identification of the whole detector by the detection of transition radiation photons.

### 3.2.3 Calorimeters

In the calorimeters all electromagnetically and strongly interacting particles (except the muons) are stopped and their energy is measured. Additionally a good position resolution is needed for particle identification.

For the inner electromagnetic calorimeter (ECAL) a high-granularity liquid-argon (LAr) sampling calorimeter in the range  $|\eta| < 3.2$  is used. It is divided into a barrel part ( $|\eta| < 1.475$ ) and two endcap components ( $1.375 < |\eta| < 3.2$ ). The ECAL is used for the identification and momentum measurements of electrons and photons. The hadronic calorimeter (HCAL) consists of three main devices. For the barrel region ( $|\eta| < 1.7$ ) a scintillator-tile calorimeter is used and in the endcap region ( $1.5 < |\eta| < 3.2$ ) a LAr hadronic calorimeter. In the forward region ( $3.1 < |\eta| < 4.9$ ) a LAr calorimeter provides both electromagnetic and hadronic energy measurements. The HCAL is used for the energy measurement of strongly interacting particles, i.e. hadrons or hadronically decaying particles (e.g. taus).

### 3.2.4 Muon Spectrometer

The outermost part of the ATLAS detector is the muon spectrometer. It measures the momentum of muons which are able to leave the detector because they pass the calorimeters with minimal energy loss. The muons are deflected in the magnetic field provided by three large superconducting air-core toroid magnets and their tracks are reconstructed using high-precision tracking chambers for a good muon momentum resolution. The tracking chambers consist of monitored drift tubes and for larger pseudorapidities ( $2.0 < |\eta| < 2.7$ ) of cathode strip chambers. Additionally to the tracking chambers the muon spectrometer also contains separate trigger chambers with high timing resolution consisting of resistive plate chambers ( $|\eta| < 1.05$ ) and thin gap chambers ( $1.05 < |\eta| < 2.4$ ).

### 3.2.5 Particle Identification

Using a combination of the information from the sub-detectors it is possible to distinguish different particles. Figure 3.3 shows a schematic overview of how particle identification is done with the ATLAS detector.



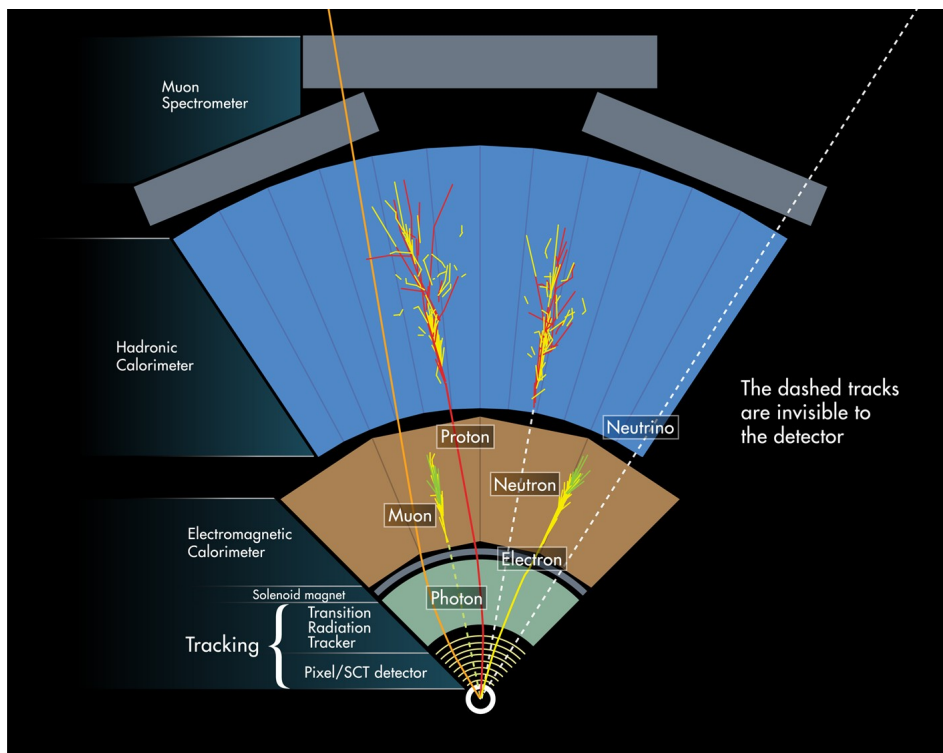


Figure 3.3: A schematic view of the ATLAS detector functions [19].

- **Protons and Neutrons** are strongly interacting and therefore leave an entry in the HCAL. Due to their charge protons also have tracks in the inner detector and in the ECAL.
- **Quarks and Gluons** are produced in many processes in a proton-proton collider. They hadronize in the detector and leave multiple tracks in the inner detector and large entries in the hadronic calorimeter (they often lose some of their energy already in the electromagnetic calorimeter). They are classified as jets and for their reconstruction sophisticated jet algorithms, for example the anti- $k_t$  algorithm [20], are used. An exception are top quarks because they are too heavy to hadronize. They decay before they can form hadrons, with nearly 100% probability into a bottom quark and a  $W$  boson.
- **$b$ -jets:** Hadrons containing a bottom quark ( $b$ -quark) have a relatively long lifetime ( $\tau_b = 1.5 \times 10^{-12}$ s), so if a  $b$ -quark is created in a collision, it forms a  $b$ -hadron and after it travels some distance it decays into a jet. Therefore the jet does not originate from the primary vertex (i.e. the collision points) but from a spatially separated secondary vertex. This information can be used to identify jets coming from a  $b$ -quark so-called  $b$ -jets. This method is called  $b$ -tagging.
- **Photons** are stopped in the ECAL and identified by an entry there with no corre-

sponding track in the inner detector.

- **Electrons** are also stopped in the ECAL, like the photons, but in contrast they must have a corresponding track in the inner detector. From this track not only the transverse momentum can be inferred, but from the curvature also the charge can be measured and electrons can be distinguished from their anti-particles, the positrons.
- **Muons** are the only charged particles which can leave the detector, since they are too heavy to be absorbed in the ECAL and they do not interact strongly. They are identified by corresponding tracks in the inner detector and the muon spectrometer. To differentiate between muons and antimuons the track curvature is used.
- **Taus** decay with a probability of about 35 % leptonically (i.e. into an electron or a muon for the tau and an antielectron or an antimuon for the antitau) and in the rest of the cases into hadrons. The former are hard to distinguish from primary electrons and muons and therefore not reconstructed as taus. The latter are easier to identify but they have to be differentiated from other strongly interacting particles. This is achieved by requiring low track multiplicity and a narrow cone of the jet.
- **Neutrinos** only interact weakly and therefore it is not possible to detect them directly in the ATLAS detector. However knowing that the initial total energy and momentum in the transverse plane is zero, the presence of neutrinos can be inferred from the missing transverse energy ( $E_T^{\text{miss}}$ ) which is defined, neglecting masses, as the absolute value of the negative sum of the transverse momenta of all visible particles  $i$  in a collision:

$$E_T^{\text{miss}} := \left| - \sum_i \vec{p}_T(i) \right|$$

A possible new particle which only interacts weakly would also contribute to the missing transverse energy.

### 3.2.6 Trigger System

Under nominal operating conditions the two proton beams in the LHC have a bunch crossing rate of roughly 30 MHz<sup>1</sup> and an average of 20 collisions per crossing. This leads to about 600 million particle collisions per second. Every collision needs approximately 1 MB disk space meaning that the ATLAS detector produces nearly 1 PB of data per second. For readout and storage reasons it is impossible to record every collision happening inside the detector. Fortunately this is not really necessary because most of the events do not contain any new or interesting physics. To determine whether a collision should be recorded (i.e. something interesting has happened) a two-level trigger system is used in the ATLAS detector. The first-level (L1) trigger is hardware-based and uses a subset of the detector

---

<sup>1</sup>The bunch spacing in the proton beams is 25 ns which would mean a bunch crossing rate of 40 MHz, but for technical reasons there are some bigger gaps in the bunch spacing of a beam reducing the bunch crossing rate.

information to reduce the rate from 30 MHz to about 100 kHz. The higher-level trigger (HLT), which is implemented in software, then brings the rate of recorded events down to approximately 1 kHz.

The L1 trigger searches for events with high transverse momentum particles or large missing transverse energy. It defines one or more regions-of-interest (RoIs), i.e. areas in the  $\eta$ - $\phi$  space where interesting features are identified. The RoIs are subsequently used by the HLT trigger. The L1 trigger only uses a limited amount of detector information to make a decision in less than 2.5  $\mu$ s.

The HLT trigger then makes use of the information from the RoI using algorithms and selection criteria similar to the offline reconstruction with an average latency of 0.2 s before it makes the final decision whether an event is recorded or not [21].

There are various trigger chains searching for different signatures in the detector. Most of the L1 trigger chains look for events where one or more objects with  $p_T$  above a certain threshold are identified. In the HLT trigger these search criteria are often refined and additional conditions can be added. The criteria have to be chosen tight enough that the rate of selected events does not exceed the rate at which they can be recorded. Trigger chains with looser conditions are used with a prescale factor  $N$ , i.e. only one event out of  $N$  events, which fulfill the selection criteria of the trigger, will be recorded.



# Chapter 4

## Data and Monte Carlo Samples

### 4.1 Data Samples

For the results shown in this thesis all data recorded in 2015 by the ATLAS detector in proton-proton collisions at a center-of-mass energy  $\sqrt{s} = 13$  TeV is used. This corresponds to an integrated luminosity  $\int L dt = 3.2 \text{ fb}^{-1}$  of good data for physics analysis, i.e. where all detector components worked acceptably during data acquisition.

### 4.2 Monte Carlo Samples

An important tool for analysis in particle physics are Monte Carlo (MC) event generators to simulate particle produced in collisions and their decay products. The simulation is in general divided into three steps [22]: generation of the events with the particle content in the initial and final states, simulation of the detector response to the particle interaction, and last the digitization of the results to get a comparable output to the readout of the ATLAS detector. The last step is needed to be able to use the same reconstruction and analysis software for real and for simulated data.

MC generators are used to simulate SM processes for background estimation and processes predicted by theoretical models such as SUSY.

To compare the MC simulations with data they need to be weighted according to their cross-section and normalized to the integrated luminosity of the recorded data. This is done with a scale factor:

$$f_{\text{MC}} = k \cdot \epsilon_{\text{filter}} \cdot \frac{(\int L dt)_{\text{data}} \sigma_{\text{MC}}}{N_{\text{MC}}}$$

with the k-factor  $k$ , the filter efficiency  $\epsilon_{\text{filter}}$ , the cross-section  $\sigma_{\text{MC}}$  of the MC process and the number of events  $N_{\text{MC}}$  in the MC sample. The k-factor is a correction factor coming from higher (next-to-leading or next-to-next-to-leading depending on the MC generator) order calculations. The filter efficiency takes into account whether all generated events

were fully simulated or if some preselection was applied at generation level (e.g only events with leptons in the final state).

### 4.2.1 Standard Model Background Samples

For this thesis most SM processes contributing to the background are estimated using MC samples. The exception is the multi-jet background which has a relative large cross-section, so it is hard to get enough statistic in the MC samples. It is also difficult to model this background correctly in the MC simulation therefore it is completely estimated from data (see Section 7). The other backgrounds are classified as  $Z$ +jets,  $W$ +jets, top and diboson.

The  $Z$ +jets and the  $W$ +jets backgrounds were simulated with Powheg-Box [23] and PYTHIA8 [24]. The top background consists of the top-antitop ( $t\bar{t}$ ) and the single top production. For both processes the Powheg-Box generator interfaced with PYTHIA6 [25] was used. The diboson processes ( $ZZ$ ,  $ZW$  and  $WW$ ) are simulated using the SHERPA generator [26].

A list of all the MC background samples used for this thesis and their k-factors, the filter efficiencies and cross-sections can be found in the Table A.2. The response of the ATLAS detector was simulated with the GEANT4 software [27] for all background samples.

### 4.2.2 SUSY Signal Samples

The two SUSY processes, chargino-antichargino ( $\tilde{\chi}_1^\pm \tilde{\chi}_1^\mp$ ) and chargino-neutralino ( $\tilde{\chi}_1^\pm \tilde{\chi}_2^0$ ) production, described in Section 2.3 are simulated as signal samples. The free parameters of these models are the masses of the  $\tilde{\chi}_1^\pm$ ,  $\tilde{\chi}_2^0$ ,  $\tilde{\chi}_1^0$ , tau-slepton ( $\tilde{\tau}_L$ ) and tau-sneutrino ( $\tilde{\nu}_\tau$ ). All other sparticles are considered to be heavy (masses of  $O(100 \text{ TeV})$ ) and therefore decoupled. Furthermore  $\tilde{\tau}_L$  and  $\tilde{\nu}_\tau$  are assumed to be mass degenerate as are  $\tilde{\chi}_1^\pm$  and  $\tilde{\chi}_2^0$ . The mass of the  $\tilde{\tau}_L/\tilde{\nu}_\tau$  is set to be halfway between the  $\tilde{\chi}_1^\pm/\tilde{\chi}_2^0$  and  $\tilde{\chi}_1^0$  mass.

For both processes the simulation was done for 73 different mass points with the  $\tilde{\chi}_1^\pm/\tilde{\chi}_2^0$  mass varied between 100 and 500 GeV and the  $\tilde{\chi}_1^0$  mass varied between 0 and 295 GeV. The condition that the  $\tilde{\chi}_1^\pm/\tilde{\chi}_2^0$  must be heavier than the  $\tilde{\chi}_1^0$  is taken into account for the simulation [28].

For the simulation MadGraph5\_aMC@NLO [29] interfaced with PYTHIA8 was used. For the signal samples the ATLAS fast calorimeter simulation [30] was used to simulate the response of the electromagnetic and hadronic calorimeter of the ATLAS detector and the GEANT4 software [27] for the response of the rest of the detector.

Several of the signal samples are combined for the closure test (see Section 6.4) to have enough statistics for a meaningful result. The list of these samples is given in the Table A.1.

# Chapter 5

## Object and Event Selection

### 5.1 Object selection

To select and identify the different objects (e.g. electrons, taus etc.) produced in the collisions, so-called physics objects are reconstructed using the information provided by the ATLAS detector. To match a physics object to a particle it has to pass certain selection criteria. But the selection criteria only give a probability that a physics object is correctly identified. It can happen that a particle is misidentified or not reconstructed at all.

The physics object needed in this analysis are electrons, muons, taus, jets,  $b$ -jets and missing transverse energy. The selection criteria of the different objects are given below and they are summarized in Table 5.1.

- **Jets** are reconstructed using the anti- $k_t$  algorithm<sup>1</sup> [20] with a distance parameter  $R = 0.4$  and topological calorimeter clusters as inputs. The reconstructed jets are calibrated taking into account several detector effects that affects the jet energy measurement. These corrections are derived from Monte Carlo simulations and from data [31].

After the corrections are applied jets are required to have a transverse momentum larger than 20 GeV and  $|\eta| < 2.8$ . A jet-vertex-tagger<sup>2</sup> (JVT) [32] value of 0.64 is required to suppress jets coming from pile-up, i.e. jets produced by additional proton-proton collisions within the same or nearby bunch-crossing.

- **$b$ -jets** are selected using a  $b$ -tagging algorithm [33] at the 77% efficiency operating point. It corresponds to a rejection factor of 140 for light jets (i.e. jets coming from gluons,  $u$ -,  $d$ - or  $s$ -quarks), of 10 for  $\tau$ -jets and of 4.5 for  $c$ -jets. They are required to have  $p_T > 20$  GeV,  $|\eta| < 2.5$  and a JVT value of 0.64.

---

<sup>1</sup>The anti- $k_t$  algorithm is a sequential clustering algorithm which produces circular cone-shaped jets, which are collinear and infrared safe.

<sup>2</sup>The jet-vertex-tagger gives a measure of how many tracks associated with a jet come from the primary vertex in an event.

- **Electrons** are reconstructed from calorimeter clusters in the ECAL and must have corresponding tracks in the inner detector. One differentiates between baseline and signal electrons. The latter have to fulfill additional and tighter selection criteria than the former.

Baseline electron candidates must have transverse momentum larger than 10 GeV,  $|\eta_{\text{cluster}}|$  smaller than 2.47 and fulfill the ‘Loose’ likelihood-based electron identification criteria described in Reference [34].

Signal electrons are required to have  $p_T > 25$  GeV and to satisfy the ‘Tight’ selection criteria [34]. They also must be isolated (using the ‘GradientLoose’ isolation working point described in Reference [34]) and fulfill two track-based cuts:  $|d_0/\sigma| < 5$  and  $|z_o \cdot \sin(\theta)| < 0.5$  mm, where  $d_0$  ( $z_o$ ) is the transverse (longitudinal) impact parameter with respect to the primary vertex,  $\sigma$  the significance of  $d_0$ , defined as the ratio of  $d_0$  and its uncertainty, and  $\theta$  the polar angle.

- **Muons** are reconstructed using information provided from the inner detector and the muon spectrometer. As the electrons, muons are also separated into baseline and signal muons.

Baseline muons are required to have  $p_T$  greater than 10 GeV,  $|\eta| < 2.5$  and to satisfy the ‘Medium’ selection criteria described in Reference [35].

Signal muons additionally must have transverse momentum larger than 25 GeV and fulfill the ‘GradientLoose’ isolation requirement [35]. Track-based cuts of  $|d_0/\sigma| < 3$  and  $|z_o \cdot \sin(\theta)| < 0.5$  mm are applied, where as for the electrons  $d_0$  ( $z_o$ ) is the transverse (longitudinal) impact parameter with respect to the primary vertex,  $\sigma$  the significance of  $d_0$  and  $\theta$  the polar angle.

- **Taus** are only labeled as such if they decay hadronically, which happens with a probability of about 65%. The tau reconstruction algorithm is seeded by a jet, reconstructed as described above but with  $p_T > 10$  GeV and  $|\eta| < 2.5$ . To reduce pile-up effects and increase the tau reconstruction efficiency a tau vertex association algorithm [36] is used to match the tau to a primary vertex candidate. Tracks from the inner detector associated to the tau candidate need to be within a cone of  $\Delta R < 0.2$  around the tau direction. The tau energy scale correction is done independently of the jet energy scale and is based on Monte Carlo simulation.

Since hadronic decays of taus are mostly characterized by the presence of one or three charged pions in addition to a neutrino and possibly neutral pions, tau candidates need to have either one or three tracks (prongs) in the inner detector with a total charge of  $\pm 1$ . Tau candidates are also required to have  $p_T > 20$  GeV and  $|\eta| < 2.47$  with the transition region between barrel and end-cap ( $1.37 < |\eta| < 1.52$ ) vetoed. They also need to satisfy the ‘Medium’ selection criteria described in Reference [36].

- The **missing transverse energy** is reconstructed using the transverse momenta of the fully calibrated and reconstructed physics objects. In addition to that also the



transverse momenta of all tracks in the inner detector originating from the primary vertex and not associated to the physics objects are used.

$$E_T^{\text{miss}} = \sqrt{(E_x^{\text{miss}})^2 + (E_y^{\text{miss}})^2}, \text{ with}$$

$$E_{x(y)}^{\text{miss}} = E_{x(y)}^{\text{miss, e}} + E_{x(y)}^{\text{miss, } \gamma} + E_{x(y)}^{\text{miss, } \tau} + E_{x(y)}^{\text{miss, jets}} + E_{x(y)}^{\text{miss, } \mu} + E_{x(y)}^{\text{miss, tracks}}$$

where the terms are the negative sum of the momenta for the respective calibrated objects [37].

<b>Jets</b>		<i>b</i> -jets
$p_T$	$p_T > 20 \text{ GeV}$	$p_T > 20 \text{ GeV}$
$\eta$ -acceptance	$ \eta  < 2.8$	$ \eta  < 2.5$
JVT	0.64	0.64
<i>b</i> -tag	-	77% operating point
<b>Electrons</b>	Baseline	Signal
$p_T$	$p_T > 10 \text{ GeV}$	$p_T > 25 \text{ GeV}$
$\eta$ -acceptance	$ \eta_{\text{cluster}}  < 2.47$	$ \eta_{\text{cluster}}  < 2.47$
quality	Loose	Tight
isolation	-	GradientLoose
track-based cuts	-	$ d_0/\sigma  < 5$ and $ z_0 \cdot \sin(\theta)  < 0.5 \text{ mm}$
<b>Muons</b>	Baseline	Signal
$p_T$	$p_T > 10 \text{ GeV}$	$p_T > 25 \text{ GeV}$
$\eta$ -acceptance	$ \eta  < 2.5$	$ \eta  < 2.5$
quality	Medium	Medium
isolation	-	GradientLoose
track-based cuts	-	$ d_0/\sigma  < 3$ and $ z_0 \cdot \sin(\theta)  < 0.5 \text{ mm}$
<b>Taus</b>		
$p_T$	$p_T > 20 \text{ GeV}$	
$\eta$ -acceptance	$ \eta  < 1.37$ or $1.52 <  \eta  < 2.47$	
n-prongs	n-prongs = 1 or 3	
charge	$ q  = 1$	
quality	Medium	

Table 5.1: Summary of the selection criteria used for the different physics objects.

## 5.2 Overlap Removal

The overlap removal (OR) procedure is used to deal with the issue of duplications, i.e. the reconstruction of one particle as two different physics objects. It also gives a handle on how to treat separate but nearby objects. As input for the overlap removal procedure the distance  $\Delta\bar{R} = \sqrt{(\bar{y}_i - \bar{y}_j)^2 + (\phi_i - \phi_j)^2}$  between two objects  $i$  and  $j$  in the  $\bar{y}$ - $\phi$  space is used (the rapidity  $\bar{y}$  has been defined in Subsection 3.2.1). The overlap removal is done in several steps in a consecutive way i.e. if an object is rejected in one step it is not used in any of the following steps. The order of the procedure is the following:

1. **Electron (Muon), Tau:** If the distance  $\Delta\bar{R}$  between a baseline electron (baseline muon) and a tau is smaller than 0.2 the tau is rejected to avoid double counting. It is more likely that an electron (muon) was correctly reconstructed than a tau.
2. **Electron, Muon:** If a baseline electron and a baseline muon share the same track in the inner detector the electron is removed to avoid duplication in the case where the muon radiates a hard photon (due to final state radiation or bremsstrahlung) and is therefore also reconstructed as an electron.
3. **Electron, Jet:** If a baseline electron and a jet have a distance less than 0.2 the jet is rejected to avoid double counting of electrons which are also reconstructed as jets. But if  $\Delta\bar{R}$  is between 0.2 and 0.4 the electron is removed. Here the electron is assumed to be produced by a semi-leptonic decay inside the jet and therefore part of it.
4. **Muon, Jet:** If the distance  $\Delta\bar{R}$  between a baseline muon and a jet is smaller than 0.4 there are two possibilities. For one a muon can radiate a hard photon (due to final state radiation or bremsstrahlung) and therefore the muon can also be reconstructed as a jet. In this case the reconstructed jet has only a small amount of tracks in the inner detector. So if the jet has less than 3 associated tracks the jet is removed. Otherwise the muon is rejected, because it is assumed to be produced by a semi-leptonic decay inside the jet.
5. **Tau, Jet:** If a tau and a jet have  $\Delta\bar{R}$  smaller than 0.2 the jet is rejected to avoid duplication because the tau reconstruction starts from a reconstructed jet.

## 5.3 Basic Event Selection

Every event needs to pass some quality requirement before it is considered for the analysis:

1. **Good-Runs-List (GRL):** The first quality requirement is only used for data and not for MC simulation. It ensures that only good data is considered (using a Good-Runs-List) meaning that only events where every detector component operated without problems during data taking are used.

2. **Good Primary Vertex:** Events need to have at least one primary vertex. This means the vertex has to be consistent with beamspot envelope and has at least two associated tracks with a transverse momentum larger than 400 MeV. If there is more than one vertex satisfying these criteria the vertex with the highest  $\sum p_T^2$  of the associated tracks is chosen.
3. **Cosmic Muon Veto:** If an event contains a cosmic muon the event is rejected. They are identified by requiring  $|z_0| > 1$  mm and  $|d_0| > 0.2$  mm for the longitudinal and transverse impact parameters with respect to the primary vertex.
4. **Bad Muon Veto:** A baseline muon is flagged as ‘bad’ if it fulfills (before the overlap removal) the equation  $\sigma(q/p)/|q/p| > 0.2$  where q is the charge and p the momentum of the track associated with the muon. The muon is badly reconstructed with a large error and therefore events containing such muons are rejected.
5. **Bad Jet Veto:** If an event contains a jet originating from detector noise or non-collision background (beam-induced background or cosmic muon showers) identified by the ‘BadLoose’ selection criteria described in Reference [38] the jet is considered badly reconstructed and the event is rejected.



# Chapter 6

## General Strategy for Measurement of Trigger Efficiencies

The main objective of this thesis is to measure the efficiency of the di-tau trigger, i.e. a trigger selecting events containing at least two hadronically decaying tau-leptons with a minimum transverse momentum of 35 GeV (25 GeV) for the first (second) tau. The di-tau trigger consists of two components, each one corresponds to a trigger which selects one tau with the respective  $p_T$ .

For the measurement of trigger efficiencies one has to distinguish between single and combined triggers. Single triggers select events containing at least one characteristic object while for combined triggers there must be at least two or more characteristic objects (depending on the specific trigger) in an event, for example the di-tau trigger is a combined trigger. In general for each component of a combined trigger there is a corresponding single trigger. If the components of a combined trigger are not correlated they can be studied independently and the efficiency of the combined trigger can be calculated from the efficiencies of the respective single triggers.

Therefore the efficiency of the di-tau trigger is determined in two steps. Firstly the efficiencies of the corresponding two single tau triggers are measured separately in data and compared to MC simulations. Secondly one needs to prove using MC simulations that the two components are not correlated so that the di-tau trigger efficiency in data can be derived from the product of the two single tau trigger efficiencies.

The naming of triggers and the specific triggers used in this thesis are explained in Section 6.1 and a general explanation how to measure trigger efficiencies is given in Section 6.2. In Section 6.3 the measurement of the efficiency for single tau triggers is described while the determination of the di-tau trigger efficiency is explained in Section 6.4.

### 6.1 Trigger Nomenclature

In this section the names of the triggers and their selection criteria are explained. As already mentioned the triggers studied are the di-tau trigger and its two corresponding

single tau triggers. Additionally for the measurement of the single tau trigger efficiencies in data a single muon trigger and two single electron triggers<sup>1</sup> are needed.

In general the naming pattern of single triggers is the following:

$$(\text{trigger level})_{\text{-(object type)}}(\text{threshold})_{\text{-(quality criteria)}}$$

where the trigger level is either L1 or HLT, the object type defines which object is selected (e.g. ‘mu’ for muon), the threshold gives the minimum  $p_T$  requirement for the selected object and the quality criteria describes which identification and/or isolation criteria the object has to fulfill. For HLT triggers it can be that the L1 trigger name, which seeded the HLT trigger, is added at the end of its name if there is some ambiguity. For combined triggers the names of the corresponding single triggers are added together after removing the trigger level between the names.

The names of the single tau triggers are ‘HLT\_tau35\_medium1\_tracktwo’ (abbreviated as Tau35) and ‘HLT\_tau25\_medium1\_tracktwo’ (abbreviated as Tau25). The Tau35/Tau25 trigger is seeded from the L1 trigger ‘L1TAU20IM’/‘L1TAU12IM’. This means for an event to pass the L1 trigger there need to be a RoI identified as an isolated (‘IM’) tau candidate with transverse momentum at first trigger level greater than 20 GeV/12 GeV. For the event to pass the HLT trigger the tau candidate is required to have  $p_T > 35$  GeV/25 GeV at HLT trigger level, between one and three tracks in the inner detector (‘tracktwo’) and must pass the online ‘medium’ identification criteria [39]. The di-tau trigger is called ‘HLT\_tau35\_medium1\_tracktwo\_tau25\_medium1\_tracktwo\_L1TAU20IM\_2TAU12IM’ and is a combination of the two single tau triggers selecting events where two taus fulfill the respective selection criteria described above.

The name of the single muon trigger is ‘HLT\_mu20\_iloose\_L1MU15’ which is the lowest unrescaled single muon trigger for the 2015 data. It selects events containing at least one muon which has a  $p_T$  at L1 greater than 15 GeV and at HLT greater than 20 GeV and a loose track isolation requirement (‘iloose’) [40].

For the electron trigger the logical ‘or’ between two unrescaled single electron triggers is used. Those two triggers are ‘HLT\_e24\_lhmedium\_L1EM20VH’ and ‘HLT\_120\_lhloose’, which is seeded from the L1 trigger ‘L1EM22VHI’. Since the L1 electron triggers only use calorimeter information (no information from the inner detector) it is not possible to distinguish between electrons and photons at that point. Therefore at L1 the object type is called ‘EM’ which stands for electromagnetic trigger. The ‘V’, ‘H’ and ‘I’ are additional quality requirements for the L1 object. ‘V’ denotes that the trigger threshold is varied as a function of the pseudorapidity to correct for the different amount of material before the calorimeter. ‘H’ indicates that a hadronic core isolation cut is applied, i.e. the energy deposit in the hadronic calorimeter behind the electromagnetic cluster of the electron candidate relative to the electromagnetic cluster energy must be less than a certain value depending on the transverse energy of the electron candidate. ‘I’ means that an

---

<sup>1</sup>One of the single electron triggers has a lower  $p_T$  threshold but tighter identification criteria while the other one has a higher  $p_T$  threshold but looser identification requirements. The second trigger is used to recover some of the efficiency of the first trigger for loose electrons with high transverse momentum.

isolation cut on the electron candidate in the ECAL is required. The ‘H’ and ‘I’ criteria are only applied for electron candidates with a transverse energy less than 50 GeV. The ‘lhmedium’/‘lhloose’ quality criteria requires that the electron pass at HLT the likelihood-based electron selection criteria ‘medium’/‘loose’ [41].

## 6.2 Trigger Efficiency: Turn-on Curves

To determine trigger efficiencies first of all an unbiased event selection is needed. Achieving an unbiased selection is more complex in data than in MC simulation (as long as there is no preselection applied for the simulation). To measure the trigger efficiency in MC samples the event selection need to contain at least the same offline reconstructed objects which are used online for the trigger decision. For example if one wishes to study a single tau trigger only events containing at least one reconstructed tau can be used. In data an additional trigger, independent<sup>2</sup> of the one studied, is needed to select events for the trigger efficiency measurement.

After applying the selection the efficiency  $\epsilon$  of a trigger then is defined as:

$$\epsilon = \frac{N_{\text{triggered}}}{N_{\text{total}}},$$

where  $N_{\text{total}}$  is the number of selected events and  $N_{\text{triggered}}$  is the number of selected events which fired the trigger (i.e. they fulfill the selection criteria of the trigger) and where the online trigger object is matched to an offline<sup>3</sup> reconstructed object of the same type. The matching is done by demanding that the distance  $\Delta R$  between the online and the offline object in the  $\eta$ - $\phi$  space is smaller than 0.2. The efficiency gives the probability for a fully reconstructed and identified offline object to pass the online trigger requirements.

Plotting the efficiency as a function of the transverse momentum of the offline object gives the turn-on curve of the trigger. Ideally the turn-on curve would be a step function where the efficiency below the trigger threshold is zero and above it the trigger is fully efficient. In general this is not the case and there is a turn-on region around the online threshold in which the efficiency increases from zero to the maximal value. The region where the trigger is fully efficient (i.e. approximately constant trigger efficiency) is called the plateau region and the offline threshold indicates at which point the plateau region starts. Figure 6.1 shows an example of such a turn-on curve. Any trigger used in an analysis to select events should be fully efficient<sup>4</sup> therefore it is important to know the offline threshold of the trigger.

---

<sup>2</sup>Independent here means that the object which fired one trigger can not be the same as the one that fired the other trigger.

<sup>3</sup>There is a difference between online and offline reconstruction. The former is done during data taking and is used as input for the trigger decision while the latter happens after the event has been recorded. Since there is only a limited amount of time to reconstruct the online variables and objects they are in general less precise than the offline ones.

<sup>4</sup>It is possible to use events in the turn-on region of a trigger, but the systematic uncertainties due to the turn-on parameterization efficiency are large and normally not worth the gain in statistics.

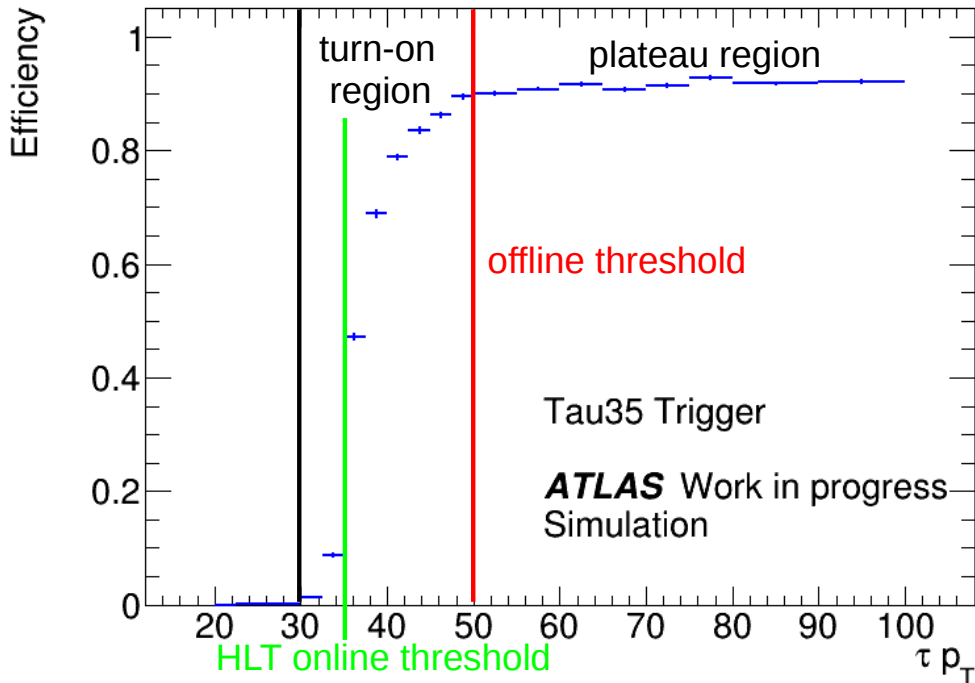


Figure 6.1: Example of a turn-on curve.

### 6.3 Single Tau Trigger Efficiency in Data: Tag-and-Probe Method

For the efficiency measurement of the tau triggers only events where the reconstructed taus are real taus and not fake ones should be used. A tau is called fake if it is actually a different physical object, mainly jets and electrons, which are wrongly reconstructed as taus. Additionally in data one needs to use a trigger to select events which must be independent of the studied trigger.

To achieve this a ‘tag-and-probe’ method is used (Figure 6.2). Events where a  $Z$  boson decays into two taus are selected. One of the taus decays further into a muon (and two neutrinos) and the other tau decays hadronically. The first tau will not be reconstructed as a tau but as a muon and can be used to tag an event, i.e. select events where an offline muon has fired a muon trigger. With the second tau the efficiency of the single tau triggers can be probed. Therefore the selected events should contain exactly one muon and one tau with opposite electrical charge (OS, short for opposite sign).

To further enhance the purity of  $Z \rightarrow \tau_{\text{had}}\tau_{\mu}$  events additional cuts are applied which are discussed in detail in Section 7.7. However it is not possible to only select  $Z \rightarrow \tau_{\text{had}}\tau_{\mu}$  events there always will be some events from other SM processes fulfilling the selection



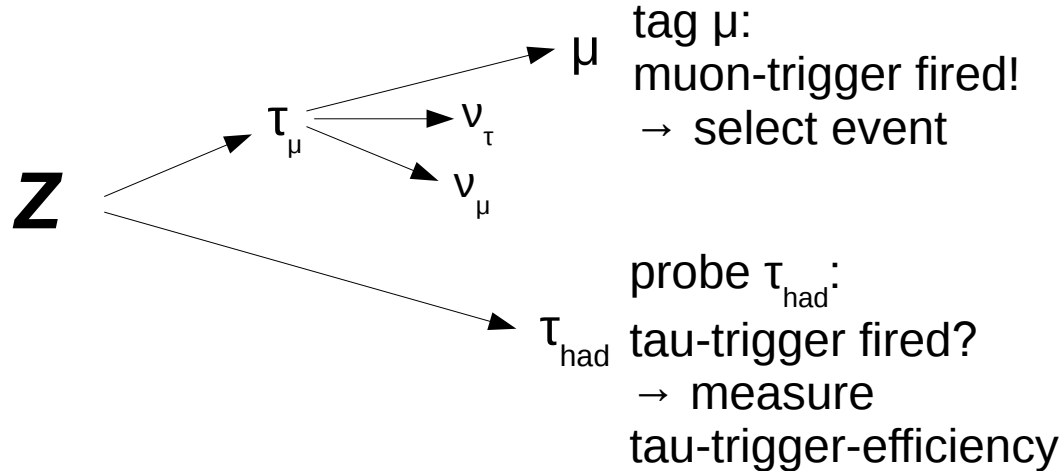


Figure 6.2: Schematic explanation of the tag-and-probe method.

cuts from data (see Chapter 7). The background contamination needs to be taken into account for the efficiency measurement (see Section 8.1)

The single tau trigger efficiencies can also be measured with the ‘tag-and-probe’ method selecting an electron instead of a muon (meaning that the first tau decays into an electron) using single electron triggers. The decay probability of the tau into an electron is slightly larger than for a muon (for electron: 17.83 % and for muon: 17.41 % [4]) but the background rejection efficiency for muons is better than for electrons. This means that there are less background events from other processes for the selection with one tau and one muon compared to the selection with one tau and one electron. Nevertheless the efficiency of the single tau triggers is measured in data for both selections in order to crosscheck the results.

For the single tau trigger efficiency in data one needs to take into account that the two considered triggers are prescaled. Prescaled means that the rate in which a trigger would select events is too high to record every event therefore only one out of  $N$  events selected by this trigger is saved.  $N$  is called the prescale factor of the trigger. In contrast to that for unprescaled triggers every event, which fulfills the selection criteria of the trigger, is recorded. Single triggers with low requirements on the transverse momentum are in general prescaled while combined triggers and single trigger with a high transverse momentum threshold or tighter identification and isolation criteria are mostly unprescaled.

To measure the efficiency of a prescaled trigger an unprescaled trigger should be used to select events in data, i.e. unprescaled single muon and electron triggers. The online information for a trigger decision is still available offline so the trigger decision of a prescaled trigger can be recomputed offline regardlessly of the fact if the event was recorded for the trigger or not. Therefore after the event selection using an unprescaled muon or electron trigger the decision of the single tau triggers is recomputed for every selected event and this result is used for the determination of the trigger efficiency.

## 6.4 Di-Tau Trigger Efficiency: Factorization and Closure Test

The di-tau trigger efficiency can be determined only in MC simulations and not from data directly. In MC simulation it is enough for the measurement of the di-tau trigger efficiency to select events containing two taus. Therefore to get a result for the efficiency in data it is assumed that if the two components of the di-tau trigger are not correlated the efficiency can be calculated by

$$\epsilon(\text{di-tau}) = \epsilon(\text{Tau35}) \cdot \epsilon(\text{Tau25}). \quad (6.1)$$

If one knows the efficiency of the single tau triggers one can also calculate the di-tau trigger efficiency. To prove this assumption a closure test using MC simulations is done. The closure  $c$  gives a measure of how correlated the components of a combined trigger are and is defined as

$$c = \frac{\epsilon(\text{di-tau})}{\epsilon(\text{Tau35}) \cdot \epsilon(\text{Tau25})}. \quad (6.2)$$

If  $c \approx 1$  the components are independent from each other and the efficiency of the di-tau trigger can be calculated as the product of the single tau triggers. The efficiencies used in the closure test are determined with MC signal samples (see Subsection 4.2.2) in order to have enough statistics for the determination of the di-tau trigger efficiency. Additionally one needs to check that the efficiency of the single tau trigger in data is approximately the same as in MC simulations, i.e. that the trigger decision is modeled correctly in the MC samples.

# Chapter 7

## Background Estimation

In order to measure the single tau trigger efficiency in data a selection containing mainly  $Z(\rightarrow \tau\tau)$  events where one tau decays hadronically and the other tau decays into a light lepton (either into a muon or an electron) is needed. The selection with a muon is called Tau-Muon channel and the one with an electron Tau-Electron channel. In both channels the selected data events are compared to the SM expectation to get an estimate of how many events are from the intended  $Z(\rightarrow \tau\tau)$  process and how many are from other processes. In the SM expectation not only the processes having the same signature (one real tau and one real muon/electron) must be taken into account but also events where one or both particles are misidentified, either because a particle was not identified correctly or another object was wrongly reconstructed as one of the particles. The SM processes can be classified into  $Z$ +jets,  $W$ +jets, top, diboson and QCD multi-jet backgrounds.

The  $Z$ +jets background consists of events where a  $Z$  boson in addition to jets is produced and the boson decays leptonically, either to electrons, muons or taus. The background can be further separated into three components depending on the lepton flavor ( $Z(\rightarrow \tau\tau)$ +jets,  $Z(\rightarrow \mu\mu)$ +jets and  $Z(\rightarrow ee)$ +jets). The background where the  $Z$  boson decays into two neutrinos is negligible and therefore not considered. Similarly in the  $W$ +jets background a  $W$  boson and jets are produced and it can also be divided into three subcategories  $W(\rightarrow \tau\nu)$ +jets,  $W(\rightarrow \mu\nu)$ +jets and  $W(\rightarrow e\nu)$ +jets. The processes where the  $Z$  or the  $W$  boson decays to quarks are also not considered. The top background is a combination from  $t\bar{t}$  events, where a top-antitop pair is produced, and single top events, where a single top is produced via the electroweak force. The diboson background contains events where two vector bosons ( $WW$ ,  $WZ$  or  $ZZ$ ) are produced and at least one of them decays leptonically. All these processes are estimated using MC simulations and in case of the  $W$ +jets background the MC simulation is normalized to data in a dedicated control region (see Section 7.4). The last background is the QCD multi-jet contribution which is estimated directly from data (see Section 7.2).

There are three control regions defined. The first one is the  $W$  control region (W-CR) which is used to check the fake tau modeling in MC simulations and to normalize the  $W$ +jets background to data. The second one is the QCD control region (QCD-CR) which is needed for the QCD multi-jet estimation and the last one is the  $Z$  control region (Z-CR)

which is the final selection used for the trigger efficiency measurements and also to check the modeling of real taus in the MC samples.

## 7.1 Trigger Scale Factors for Light Lepton Triggers

To take into account potential differences in the efficiencies of the muon and electron triggers between data and MC simulations scale factors are used to adjust the events from the MC samples. The trigger scale factors are derived from the ratio of the trigger efficiencies in data and Monte Carlo simulations from  $Z \rightarrow ee$  or  $Z \rightarrow \mu\mu$  events depending on the trigger.

This is especially important for the electron trigger ‘HLT\_e24\_lhmedium\_L1EM20VH’ since the decision of this trigger is not available in the MC samples so instead the trigger ‘HLT\_e24\_lhmedium\_L1EM18VH’ is used and the difference between those two is corrected by the scale factors.

## 7.2 Multi-Jet and General Background Estimation

The multi-jet background has a relative high cross-section and it is difficult to model it correctly in MC simulation, therefore it is estimated from data. For the estimation the ‘OS-SS’ method is used, similar to what is done in Reference [42]. To estimate the multi-jet contribution for the different control regions events which fulfill all selection criteria for that particular CR are used except that the light lepton and the tau are required to have the same electrical charge (SS) rather than the opposite one (OS).

Two assumptions are made to estimate the multi-jet contribution in such a way. The first one is that the multi-jet background for the opposite sign events is equal to the multi-jet contribution with same sign events which is scaled with a factor called  $r_{\text{QCD}}$ , implying that the shape of the OS contribution is the same as for the SS contribution. This is assumed for all control regions:

$$\text{multi-jet(OS)} = r_{\text{QCD}} \cdot \text{multi-jet(SS)}. \quad (7.1)$$

The factor  $r_{\text{QCD}}$  is derived from the QCD-CR, separately for the Tau-Muon and the Tau-Electron channel. The QCD-CR is chosen in such a way that mainly events from the multi-jet background are selected (see Section 7.5), meaning that the contributions from other processes (i.e.  $Z$ +jets,  $W$ +jets, top and diboson) estimated with MC simulations are small. The factor  $r_{\text{QCD}}$  is defined as

$$r_{\text{QCD}} = \frac{\text{multi-jet(OS)}}{\text{multi-jet(SS)}} \Bigg|_{\text{QCD-CR}} = \frac{\text{data(OS)-MC}^{\text{other}}(\text{OS})}{\text{data(SS)-MC}^{\text{other}}(\text{SS})} \Bigg|_{\text{QCD-CR}} \quad (7.2)$$

where the superscript ‘other’ stresses that the multi-jet QCD events are not part of the MC simulated background samples. The scale factor takes into account the potential

differences between OS and SS multi-jet events coming from the final state jets which were misidentified as the tau and the light lepton.

The second assumption is that one gets the SS multi-jet contribution in all control regions from the difference between the same sign data and MC events in the specific control region:

$$\text{multi-jet(SS)} = \text{data(SS)} - \text{MC}^{\text{other}}(\text{SS}) \quad (7.3)$$

That means if one subtracts from the same sign data events all same sign MC simulated SM processes ( $Z$ +jets,  $W$ +jets, top and diboson) what is left is the multi-jet background in the SS region. This implies that  $\text{MC}^{\text{other}}(\text{SS})$  should be small compared to  $\text{data}(\text{SS})$ . Therefore the mis-modeling in MC simulation can be neglected and it also implies that SM events other than multi-jet do not contribute to the SS region after subtracting the MC same sign events.

Using Equation 7.1 and 7.3 the multi-jet contribution in the opposite sign region is:

$$\text{multi-jet(OS)} = r_{\text{QCD}}(\text{data(SS)} - \text{MC}^{\text{other}}(\text{SS})) = r_{\text{QCD}} \cdot \text{data(SS)} - r_{\text{QCD}} \cdot \text{MC}^{\text{other}}(\text{SS}) \quad (7.4)$$

Since the multi-jet background is calculated from a difference it can happen that it gets a negative prediction due to statistical fluctuations, especially if the multi-jet contribution is small. This can either be the case for a whole control region if it is chosen in such a way that it contains nearly no multi-jet events or for some of the bins in the histograms of the kinematic distributions. To minimize those negative predictions while plotting the kinematic distributions the MC same sign events are not directly subtracted from the data same sign events but instead they are subtracted from the corresponding MC opposite sign events. Therefore the SM contribution for the comparison with the opposite sign data events is estimated by:

$$\begin{aligned} \text{data(OS)} &= r_{\text{QCD}} \cdot \text{data(SS)} + \sum_{\text{MC}} (\text{MC}^{\text{other}}(\text{OS}) - r_{\text{QCD}} \cdot \text{MC}^{\text{other}}(\text{SS})) \\ &= r_{\text{QCD}} \cdot \text{data(SS)} + (Z^{\text{MC}}(\text{OS}) - r_{\text{QCD}} \cdot Z^{\text{MC}}(\text{SS})) \\ &\quad + (k_{\text{W}}^{\text{OS}} W^{\text{MC}}(\text{OS}) - r_{\text{QCD}} \cdot k_{\text{W}}^{\text{SS}} W^{\text{MC}}(\text{SS})) \\ &\quad + (\text{top}^{\text{MC}}(\text{OS}) - r_{\text{QCD}} \cdot \text{top}^{\text{MC}}(\text{SS})) + (\text{diboson}^{\text{MC}}(\text{OS}) - r_{\text{QCD}} \cdot \text{diboson}^{\text{MC}}(\text{SS})) \\ &= r_{\text{QCD}} \text{data(SS)} + Z^{\text{MC}}(\text{OS-rSS}) + W^{\text{MC}}(\text{OS-rSS}) + \text{top}^{\text{MC}}(\text{OS-rSS}) \\ &\quad + \text{diboson}^{\text{MC}}(\text{OS-rSS}), \end{aligned} \quad (7.5)$$

where ‘OS-rSS’ is a shortened form to describe that the scaled same sign events are subtracted from the opposite sign events. There can still be negative contributions in some of the bins of the kinematic distributions for the MC backgrounds if the opposite sign event contribution is smaller than the scaled same sign contribution. This may be if

there is no correlations between the charge of the reconstructed tau and the reconstructed light lepton. If that is the case the content of the corresponding bin of the respective MC background is set to zero.

The  $W$ +jets background is scaled with a factor  $k_W^{\text{OS}}$  for the opposite sign region and with a factor  $k_W^{\text{SS}}$  for the same sign region. This is done to take into account potential differences between data and MC simulation in the fake tau modeling. In the  $W$ +jets background the muon comes from the decay of the  $W$  boson and the tau is wrongly reconstructed from a jet and therefore fake. The scale-factors are calculated in the W control region (see Section 7.4), a region where mainly events from the  $W$ +jets background, more specific from the  $W(\rightarrow \mu\nu)$ +jets ( $W(\rightarrow e\nu)$ +jets) background for the Tau-Muon (Tau-Electron) channel, are selected. The scale-factors are calculated separately for both channels with:

$$k_W^{\text{OS}} = \frac{\text{data}(\text{OS}) - (Z^{\text{MC}}(\text{OS}) + \text{top}^{\text{MC}}(\text{OS}) + \text{diboson}^{\text{MC}}(\text{OS}))}{W^{\text{MC}}(\text{OS})} \Bigg|_{\text{W-CR}} \quad (7.6)$$

$$k_W^{\text{SS}} = \frac{\text{data}(\text{SS}) - (Z^{\text{MC}}(\text{SS}) + \text{top}^{\text{MC}}(\text{SS}) + \text{diboson}^{\text{MC}}(\text{SS}))}{W^{\text{MC}}(\text{SS})} \Bigg|_{\text{W-CR}} \quad (7.7)$$

The multi-jet contribution is small in the W-CR and neglected for the determination of the scale-factors.

In the following the three control regions are define and the results of the comparison between data and the estimated SM expectations are shown for each CR. In Section 7.3 the preselection which is applied to all the control regions is presented. The section about the W-CR is split in two parts. In the first part (Section 7.4) the scale factors  $k_W^{\text{OS}}$  and  $k_W^{\text{SS}}$  are calculated and it is shown that the multi-jet contribution can be neglected for that calculation. In Section 7.5 the QCD-CR is discussed and the scale factor  $r_{\text{QCD}}$  is determined. The factor  $r_{\text{QCD}}$  is needed for the second part of the W-CR (Section 7.6), which shows the result of the SM expectation while not neglecting the multi-jet contribution (using Equation 7.5). Finally the Z-CR is discussed in Section 7.7.

## 7.3 Preselection

The selection described in this section is applied for all three control regions. It is summarized in Table 7.1.

### 7.3.1 Tau-Muon Selection

In the Tau-Muon channel as already mentioned before one selects events which have exactly one tau and one muon with opposite sign. The muon must pass the baseline selection criteria described in Section 5.1. The events should also not contain a baseline electron and need to fulfill the quality requirements detailed in Section 5.3. The offline muon

must have fired the single muon trigger ‘HLT\_mu20\_loose\_L1MU15’<sup>1</sup>. Additionally the transverse momentum of the muon needs to be larger than 22 GeV to be in the plateau region of the muon trigger.

### 7.3.2 Tau-Electron Selection

In the Tau-Electron channel events containing exactly one tau and one baseline electron with opposite sign are selected. They too must pass the quality requirements from Section 5.3 and there should be no baseline muon. At least one of the two electron triggers ‘HLT\_e24\_lhmedium\_L1EM20VH’ or ‘HLT\_120\_lhloose’ must have fired and the offline electron must be matched to a corresponding online electron and the transverse momentum of the baseline electron is required to be bigger than 25 GeV.

Preselection:	
Tau-Muon channel:	Tau-Electron channel:
good event quality (see Section 5.3)	good event quality (see Section 5.3)
single muon trigger fired	single electron trigger fired
exactly one baseline muon	exactly one baseline electron
$p_T(\mu) > 22 \text{ GeV}$	$p_T(e) > 25 \text{ GeV}$
offline muon is matched to online muon	offline electron is matched to online electron
exactly one tau	exactly one tau
electron veto	muon veto
muon and tau have opposite sign	electron and tau have opposite sign

Table 7.1: Preselection for the Tau-Muon and Tau-Electron channel applied to all three control regions.

## 7.4 W Control Region: Scale Factors $k_W^{\text{OS}}$ and $k_W^{\text{SS}}$

In this section the W-CR is defined and the two scale factors  $k_W^{\text{OS}}$  and  $k_W^{\text{SS}}$  are calculated and it is shown that the results are valid despite neglecting the multi-jet contribution.

For the W control region mainly events from the  $W(\rightarrow \mu\nu)+\text{jets}$  background for the Tau-Muon and from the  $W(\rightarrow e\nu)+\text{jets}$  background for the Tau-Electron channel should be selected. In this region the light lepton comes from the W boson decay and the tau is a wrongly reconstructed jet. As a consequence of that the modeling of fake taus in MC simulations can be checked by comparing data and SM expectation. Potential differences between MC and data are taken into account by calculating scale factors for the

<sup>1</sup>This means that the offline muon is matched to an online muon which passes the trigger selection criteria. The condition for a match is that the distance  $\Delta R$  in the  $\eta$ - $\phi$  space between online and offline muon is smaller than 0.2

$W$ +jets background in the opposite and same sign region separately for both channels (cf. Equation 7.6 and 7.7).

For the selection in both channels the events have to pass the respective preselection defined in Section 7.3. The selected light lepton must fulfill the criteria of the corresponding signal lepton (see Section 5.1) to reject most of the multi-jet background. The light lepton for the  $W$ +jets background comes from the decay of the  $W$  boson and is in general isolated, and therefore identified as a signal lepton in contrast to the multi-jet background where the condition of isolation is normally not fulfilled. To further suppress the multi-jet background and to discriminate against the  $Z(\rightarrow \tau\tau)$ +jets background (and in case of the Tau-Electron channel also against the  $Z(\rightarrow ee)$ +jets contribution) the transverse mass  $m_T$  of the light lepton and the  $E_T^{\text{miss}}$  should be bigger than 50 GeV and the  $E_T^{\text{miss}}$  in an event larger than 20 GeV. The transverse mass  $m_T(\ell, E_T^{\text{miss}})$  with  $\ell = \mu, e$  is an important variable to select  $W \rightarrow e\nu/\mu\nu$  events (or to discriminate against them in the other control regions) and is defined as:

$$m_T(\ell, E_T^{\text{miss}}) = \sqrt{2 \cdot p_T(\ell) \cdot E_T^{\text{miss}} \cdot (1 - \cos(\Delta\phi(\ell, E_T^{\text{miss}})))}$$

For the  $W$ +jets background most of the  $E_T^{\text{miss}}$  comes from the neutrino and the transverse mass has a peak at about the value of the  $W$  boson mass. In contrast to that in the multi-jet and the  $Z$ +jets events lower values of  $m_T$  are expected. To suppress the top background a  $b$ -jet veto is applied, i.e. an event is not allowed to contain a  $b$ -jet. The selection cuts for the  $W$ -CR are summarized in Table 7.2.

Tau-Muon W-CR selection:	Tau-Electron W-CR selection:
Tau-Muon preselection	Tau-Electron preselection
muon is signal muon	electron is signal electron
$m_T(\mu, E_T^{\text{miss}}) > 50 \text{ GeV}$	$m_T(e, E_T^{\text{miss}}) > 50 \text{ GeV}$
$E_T^{\text{miss}} > 20 \text{ GeV}$	$E_T^{\text{miss}} > 20 \text{ GeV}$
$b$ -jet veto	$b$ -jet veto

Table 7.2: Definition of the Tau-Muon and Tau-Electron  $W$  control region.

The number of events from MC and data passing the selection for the opposite and same sign region are given in Table 7.3 for both channels. In the table the event yields of the  $W$ +jets backgrounds are already scaled with  $k_W^{\text{OS}}$  and  $k_W^{\text{SS}}$ . The scale factors are calculated with Equation 7.6 and 7.7 using the event yield before the  $W$ +jets contributions are rescaled. The multi-jet background is assumed to be small in the  $W$ -CR and is not considered for the calculation. The reason for calculating the scale factors is the assumption that the differences between data and SM expectation in the  $W$ -CR come from the MC mis-modeling of fake taus in the  $W$ +jets background. The OS region is dominated by fake taus from quark initiated jets, which are charge correlated with the lepton from the  $W$  boson decay, whereas in the SS region the fake tau comes from both gluon and quark jets. This is the reason why the scale factors are calculated separately for the OS and the SS region. The



resulting scale factors for both selections are shown in Table 7.4. The difference between the two channels can be explained by differing reconstruction and selection efficiencies of the muon and the electron. The purity (i.e. the ratio between the  $W$ +jets backgrounds events and the data events) for the W-CR selection in the OS region is larger than 85% for both channels after applying the scale factors.

Sample:	Tau-Muon selection:		Tau-Electron selection:	
	OS	SS	OS	SS
$Z \rightarrow ee$ :	$0 \pm 0$	$0 \pm 0$	$2420 \pm 32$	$513 \pm 15$
$Z \rightarrow \mu\mu$ :	$917 \pm 20$	$770 \pm 18$	$0 \pm 0$	$0 \pm 0$
$Z \rightarrow \tau\tau$ :	$1720 \pm 27$	$54 \pm 5$	$1390 \pm 24$	$42 \pm 4$
$W \rightarrow e\nu$ :	$0 \pm 0$	$0 \pm 0$	$39000 \pm 500$	$19500 \pm 400$
$W \rightarrow \mu\nu$ :	$37100 \pm 500$	$17480 \pm 350$	$5 \pm 3.5$	$3.1 \pm 3.1$
$W \rightarrow \tau\nu$ :	$680 \pm 40$	$326 \pm 28$	$790 \pm 40$	$399 \pm 34$
$t\bar{t}$ :	$693 \pm 8$	$180 \pm$	$826 \pm 9$	$221 \pm 5$
single top:	$194.8 \pm 2.4$	$67.4 \pm 1.5$	$223.4 \pm 2.7$	$74.8 \pm 1.6$
Diboson:	$578 \pm 5$	$117.7 \pm 2.6$	$627 \pm 5$	$123.5 \pm 2.6$
total MC:	$41900 \pm 500$	$19000 \pm 350$	$45300 \pm 500$	$20900 \pm 400$
data:	41892	18995	45270	20876

Table 7.3: MC and data event yields in the W-CR for the Tau-Muon and Tau-Electron selection in the opposite sign and the same sign region. The  $W$ +jets backgrounds are scaled with  $k_W^{\text{OS/SS}}$ . The uncertainties represent the statistical errors.

Tau-Muon selection:		Tau-Electron selection:	
$k_W^{\text{OS}}$	$k_W^{\text{SS}}$	$k_W^{\text{OS}}$	$k_W^{\text{SS}}$
$1.119 \pm 0.012$	$1.366 \pm 0.021$	$1.380 \pm 0.013$	$1.712 \pm 0.024$

Table 7.4: The scale factors  $k_W^{\text{OS}}$  and  $k_W^{\text{SS}}$  for the Tau-Muon and Tau-Electron selection calculated from the event yields in the W-CR. The uncertainties represent the statistical errors.

To check the assumption of a small multi-jet background and therefore that it can be neglected for the calculation of  $k_W^{\text{OS/SS}}$  some kinematic variables are plotted for the opposite sign and the same sign region without the multi-jet estimation described in Section 7.2. In the plots only the events from the MC simulated samples are used, where the  $W$ +jets background is scaled with  $k_W^{\text{OS}}$  and  $k_W^{\text{SS}}$  respectively and these events are compared to the opposite sign and same sign events in data.

In Figure 7.1 and Figure 7.2 the distributions of the  $E_T^{\text{miss}}$  and of the transverse momentum of the light lepton for both channel in the OS region are shown. Figure 7.3 and Figure 7.4 show the same for the SS region. A good agreement between the MC estimation

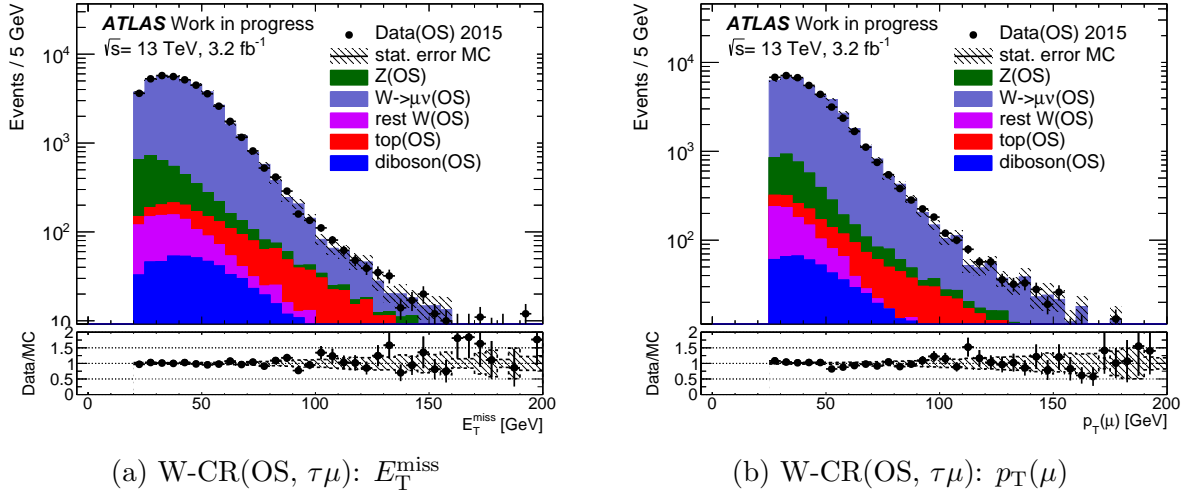


Figure 7.1: The measured  $E_T^{\text{miss}}$  (left) and  $p_T(\mu)$  (right) distributions of the opposite sign events in the W-CR for the Tau-Muon channel. The  $W$ +jets background is scaled with  $k_W^{\text{OS}}$  and the multi-jet background is neglected. The hatched bands represent the statistical error of the MC expectation. The lower panels show the ratio between data and MC expectation.

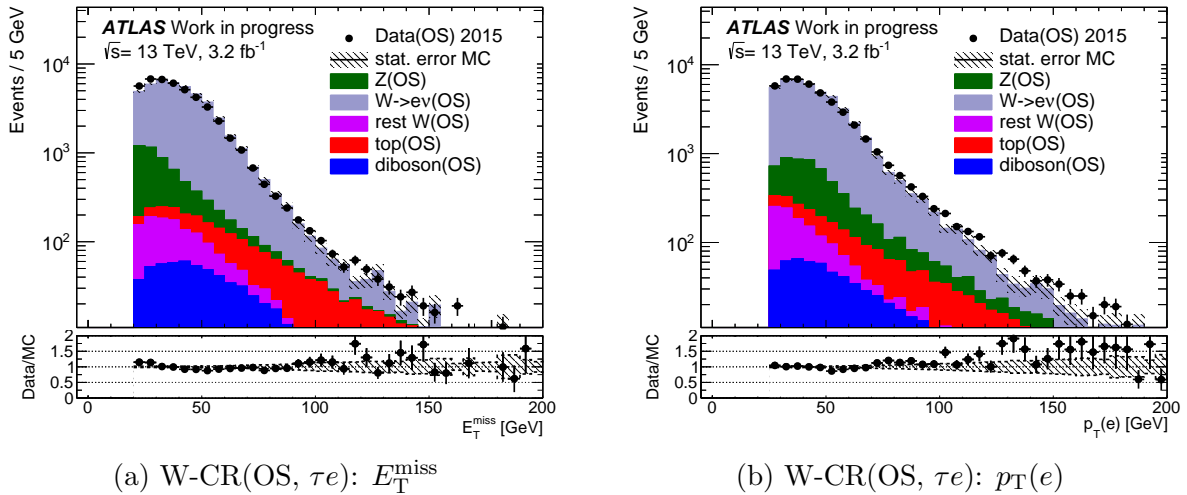


Figure 7.2: The measured  $E_T^{\text{miss}}$  (left) and  $p_T(e)$  (right) distributions of the opposite sign events in the W-CR for the Tau-Electron channel. The  $W$ +jets background is scaled with  $k_W^{\text{OS}}$  and the multi-jet background is neglected. The hatched bands represent the statistical error of the MC expectation. The lower panels show the ratio between data and MC expectation.

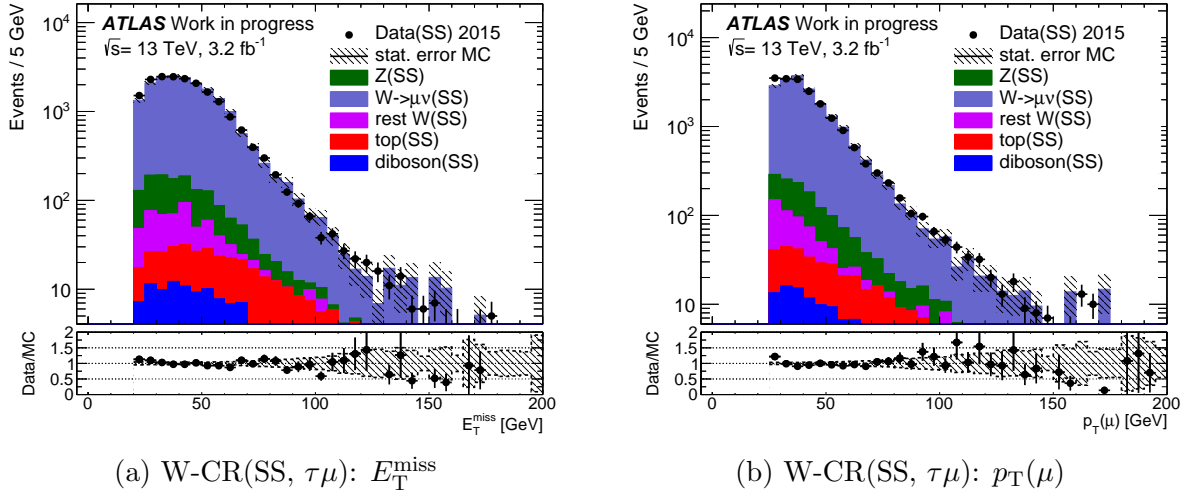


Figure 7.3: The measured  $E_T^{\text{miss}}$  (left) and  $p_T(\mu)$  (right) distributions of the same sign events in the W-CR for the Tau-Muon channel. The  $W$ +jets background is additionally scaled with  $k_W^{\text{SS}}$  and the multi-jet background is neglected. The hatched bands represent the statistical error of the MC expectation. The lower panels show the ratio between data and MC expectation.

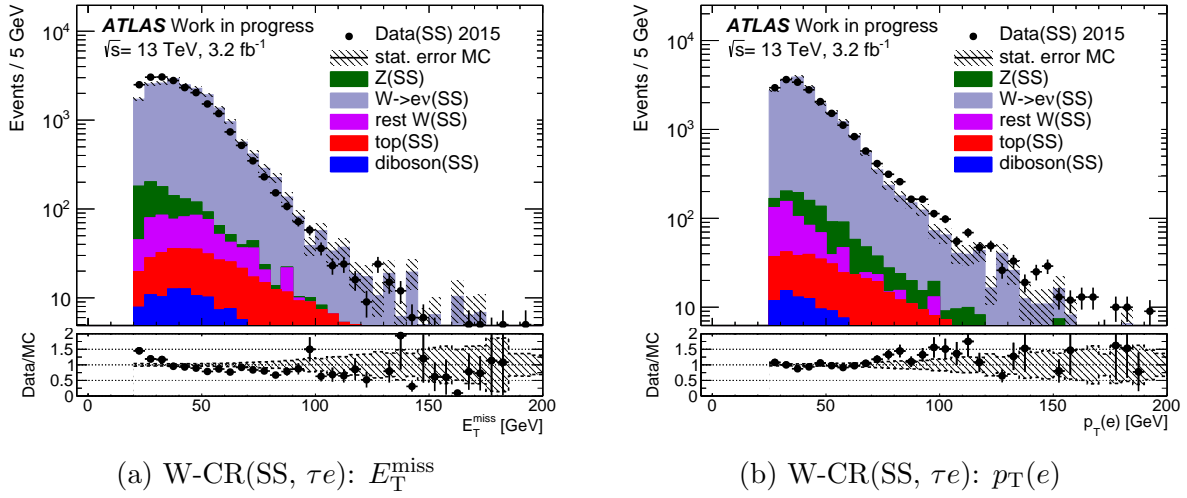


Figure 7.4: The measured  $E_T^{\text{miss}}$  (left) and  $p_T(e)$  (right) distributions of the same sign events in the W-CR for the Tau-Electron channel. The  $W$ +jets background is additionally scaled with  $k_W^{\text{SS}}$  and the multi-jet background is neglected. The hatched bands represent the statistical error of the MC expectation. The lower panels show the ratio between data and MC expectation.

and the data is observed. There are some fluctuations in the distributions at higher values of the transverse momentum and the missing transverse energy, but they are mostly within the statistical errors. Also in the OS region for the Tau-Electron channel at low  $E_T^{\text{miss}}$  (between 20 GeV and 30 GeV) there is a discrepancy between data and the MC expectation of around 10 %. This is even more pronounced in the SS region. It can be explained by the fact that the multi-jet contribution in the Tau-Electron channel in general is larger than in the Tau-Muon channel and that therefore it also has a higher contribution in the W-CR. The multi-jet background is still quite small in the Tau-Electron channel but it is higher than in the Tau-muon channel.

To take the multi-jet background into account the scale factor  $r_{\text{QCD}}$  is needed which is calculated in the QCD-CR. Therefore the QCD control region is discussed in the next section before the results for the W-CR with the multi-jet contribution are shown.

## 7.5 QCD control region

The QCD control region should mainly contain multi-jet events. The events in the Tau-Muon and the Tau-Electron channel again need to pass the respective preselection described in Section 7.3. Additionally to that the selected muon (electron) is not allowed to be a signal muon (electron)(see Section 5.1). Since in the multi-jet background the light lepton comes either from a wrongly reconstructed jet or from a semi-leptonic decay in a jet demanding that the light lepton is not a signal muon/electron will mostly select multi-jet events. Also the transverse mass between the light lepton and the missing transverse energy in an event must be smaller than 50 GeV to reject  $W$ +jets events. The selection cuts for the QCD-CR are summarized in Table 7.5.

Tau-Muon QCD-CR selection:	Tau-Electron QCD-CR selection:
Tau-Muon preselection	Tau-Electron preselection
muon is not signal muon	electron is not signal electron
$m_T(\mu, E_T^{\text{miss}}) < 50 \text{ GeV}$	$m_T(e, E_T^{\text{miss}}) < 50 \text{ GeV}$

Table 7.5: Definition of the Tau-Muon and Tau-Electron QCD control region.

After applying these cuts the number of selected events for data and the processes estimated with MC simulations in the opposite sign and the same sign region for both channels are given in Table 7.6. The total MC events are less than 15 % of the data events in the OS region for the Tau-Muon and about 10 % for the Tau-Electron channel. It is assumed that in the SS region the difference between the MC and data events is the multi-jet background (cf. Equation 7.3) and in the QCD-CR the same applies for the OS events (cf. Equation 7.2 and 7.4). Therefore the purity of the QCD-CR is more than 85 % for both channels. The purity here is defined as the number of multi-jets events divided by the number of data events in the opposite sign region.

Sample:	Tau-Muon selection:		Tau-Electron selection:	
	OS	SS	OS	SS
$Z \rightarrow ee$ :	$0 \pm 0$	$0 \pm 0$	$2593 \pm 34$	$483 \pm 15$
$Z \rightarrow \mu\mu$ :	$46 \pm 5$	$32 \pm 4$	$0 \pm 0$	$0 \pm 0$
$Z \rightarrow \tau\tau$ :	$4260 \pm 40$	$75 \pm 6$	$3700 \pm 40$	$195 \pm 9$
$W \rightarrow e\nu$ :	$0 \pm 0$	$0 \pm 0$	$1600 \pm 70$	$1030 \pm 60$
$W \rightarrow \mu\nu$ :	$398 \pm 33$	$188 \pm 24$	$0 \pm 0$	$0 \pm 0$
$W \rightarrow \tau\nu$ :	$375 \pm 29$	$125 \pm 18$	$345 \pm 30$	$188 \pm 24$
$t\bar{t}$ :	$236 \pm 5$	$57.6 \pm 2.8$	$392.2 \pm 10$	$155 \pm 7$
single top:	$25.9 \pm 0.9$	$8.1 \pm 0.5$	$47.2 \pm 1.2$	$18.9 \pm 0.8$
Diboson:	$35.3 \pm 1.7$	$6.4 \pm 0.6$	$52.5 \pm 1.9$	$14.1 \pm 0.9$
total MC:	$5380 \pm 60$	$492 \pm 31$	$8740 \pm 90$	$2090 \pm 70$
data:	36422	21789	83747	70960

Table 7.6: MC and data event yields in the QCD-CR for the Tau-Muon and Tau-Electron selection for the opposite sign and the same sign region. The  $W$ +jets backgrounds are scaled with  $k_W^{\text{OS/SS}}$ . The uncertainties represent the statistical errors.

In the Tau-Electron channel the number of selected events are more than two times the amount of the Tau-Muon channel. This is be explained by the fact that it is more probable that a jet is wrongly reconstructed as an electron than as a muon.

Using the event yields from Table 7.6 and Equation 7.2 the scale factor  $r_{\text{QCD}}$  for the Tau-Muon and Tau-Electron selection is calculated. The resulting values are approximately 1.5 for the former and 1.1 for the latter (see Table 7.7).

$r_{\text{QCD}}$ for Tau-Muon selection:	$r_{\text{QCD}}$ for Tau-Electron selection:
$1.458 \pm 0.014$	$1.089 \pm 0.006$

Table 7.7: The scale factor  $r_{\text{QCD}}$  for the Tau-Muon and Tau-Electron selection calculated from the event yields in the QCD-CR. The uncertainties represent the statistical errors.

The event yields for the QCD-CR are shown in Table 7.8. The SS events in data and MC are scaled with  $r_{\text{QCD}}$  and the latter are subtracted from the corresponding OS events. The  $W$ +jets background is scaled with  $k_W^{\text{OS}}$  in the opposite sign region and with  $k_W^{\text{SS}}$  in the same sign region.

As expected a good agreement between the total number of the opposite sign data events and the SM contribution is observed in the QCD-CR. To check that also the shape of different kinematic variables is in agreement, the missing transverse energy and the transverse momentum of the light lepton of the selected events are shown in Figure 7.5 for the Tau-Muon channel and in Figure 7.6 for the Tau-Electron channel. A good agreement between SM expectation and data is observed. The small bump in the distribution of the transverse momentum of the electron (Figure 7.6b) above 120 GeV is explained by

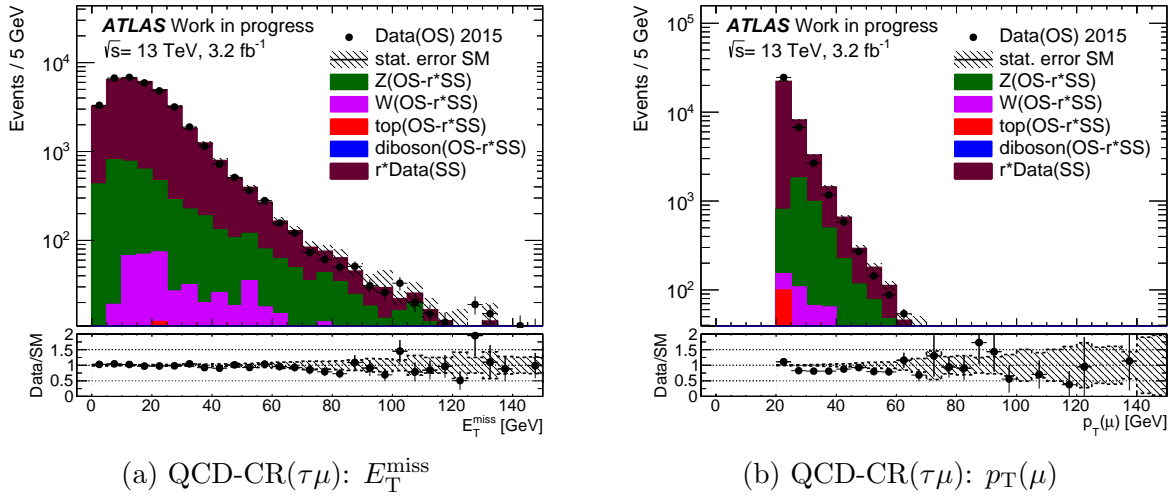


Figure 7.5: The measured  $E_T^{\text{miss}}$  (left) and  $p_T(\mu)$  (right) distributions in the QCD-CR for the Tau-Muon channel. The same sign data and MC events are scaled with  $r_{\text{QCD}}$  before the latter are subtracted from the corresponding opposite sign MC events. The  $W$ +jets background is additionally scaled with  $k_W^{\text{OS/SS}}$ . The hatched bands represent the statistical error of the SM expectation. The lower panels show the ratio between data and SM expectation.

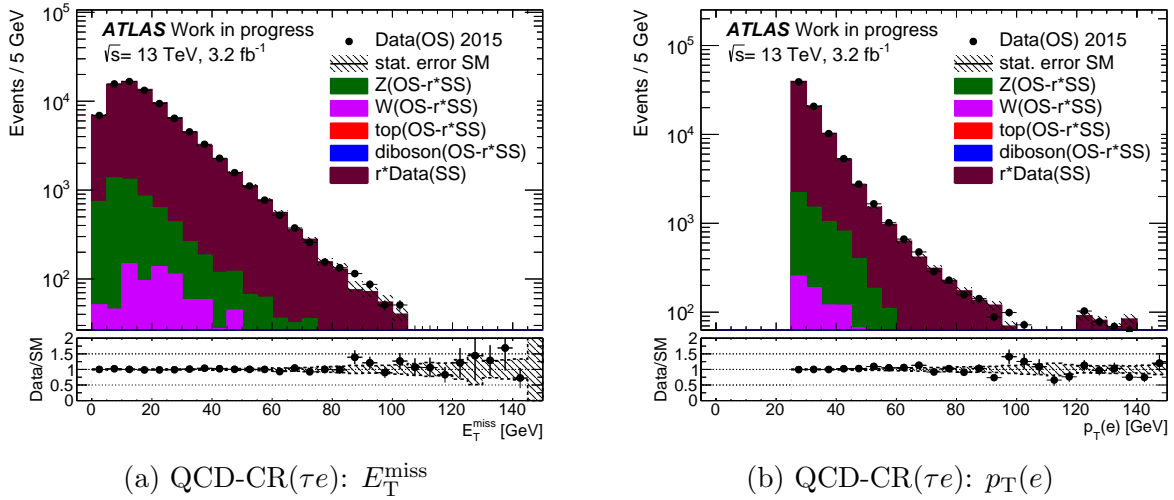


Figure 7.6: The measured  $E_T^{\text{miss}}$  (left) and  $p_T(e)$  (right) distributions in the QCD-CR for the Tau-Electron channel. The same sign data and MC events are scaled with  $r_{\text{QCD}}$  before the latter are subtracted from the corresponding opposite sign MC events. The  $W$ +jets background is additionally scaled with  $k_W^{\text{OS/SS}}$ . The hatched bands represent the statistical error of the SM expectation. The lower panels show the ratio between data and SM expectation.

Sample	Tau-Muon selection:	Tau-Electron selection:
$Z \rightarrow ee$ : OS-rSS	$0 \pm 0$	$2070 \pm 40$
$Z \rightarrow \mu\mu$ : OS-rSS	$0 \pm 7$	$0 \pm 0$
$Z \rightarrow \tau\tau$ : OS-rSS	$4150 \pm 40$	$3490 \pm 40$
$W \rightarrow e\nu$ : OS-rSS	$0 \pm 0$	$480 \pm 90$
$W \rightarrow \mu\nu$ : OS-rSS	$120 \pm 50$	$0 \pm 0$
$W \rightarrow \tau\nu$ : OS-rSS	$190 \pm 40$	$140 \pm 40$
$t\bar{t}$ : OS-rSS	$152 \pm 6$	$223 \pm 13$
single top: OS-rSS	$14 \pm 1.2$	$26.5 \pm 1.5$
Diboson: OS-rSS	$26 \pm 1.9$	$37.1 \pm 2.2$
r*Data(SS)	$31800 \pm 400$	$77300 \pm 500$
total SM:	$36400 \pm 400$	$83800 \pm 500$
Data(OS):	36422	83747

Table 7.8: Event yields in the QCD-CR for the Tau-Muon and Tau-Electron selection after subtracting the with  $r_{\text{QCD}}$  scaled SS events from the OS events. The  $W$ +jets backgrounds are also scaled with  $k_{\text{W}}^{\text{OS/SS}}$ . The uncertainties represent the statistical errors.

the second electron trigger ‘HLT\_120\_lhloose’, which has a looser selection criteria for the electron quality.

## 7.6 W Control Region: Background Estimation

Since the factor  $r_{\text{QCD}}$  was determined in the section before the results for the W-CR using the background estimation method described in Section 7.2 are shown in this section, therefore also taking the multi-jet background into account. The event yields for that are shown in Table 7.9. The SS events in data and MC are scaled with  $r_{\text{QCD}}$  and the latter are then subtracted from the corresponding OS events. The  $W$ +jets background is scaled with  $k_{\text{W}}^{\text{OS}}$  in the opposite sign region and with  $k_{\text{W}}^{\text{SS}}$  in the same sign region. The rather low number of  $W$ +jets events and the high number of data same sign events comes from the fact, that there are quite a lot MC same sign events for the  $W$ +jets background. These SS events are subtracted from the  $W$ +jets OS events, therefore reducing them quite a lot. But this is taken into account with the SS data events which for the W-CR contain mainly those  $W$ +jets SS events and not multi-jet events.

Due to the rescaling of the  $W$ +jets backgrounds it is expected that the total number of the opposite sign data events and the SM expectation agree with each other. By plotting some kinematic variables for the W-CR selection it can be checked if the shape of them also agrees, now considering all background processes. This is shown in Figure 7.7 for the Tau-Muon and in Figure 7.8 for the Tau-Electron selection for the distribution of  $E_{\text{T}}^{\text{miss}}$  and the muon/electron transverse momentum respectively. Within the statistical

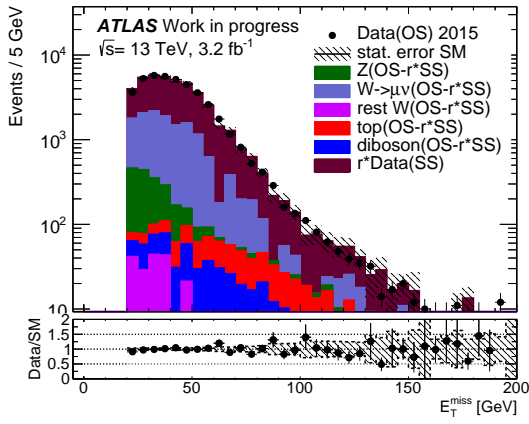
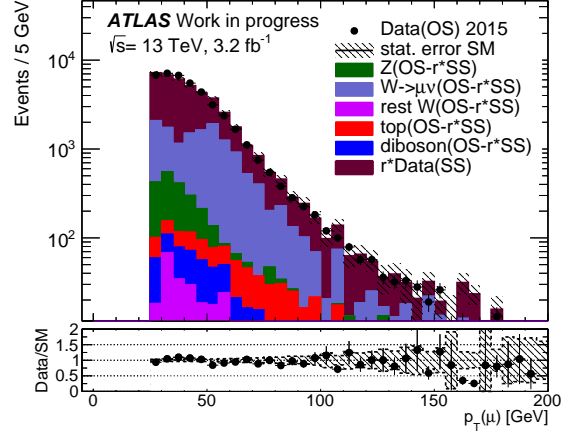
(a) W-CR( $\tau\mu$ ):  $E_T^{\text{miss}}$ (b) W-CR( $\tau\mu$ ):  $p_T(\mu)$ 

Figure 7.7: The measured  $E_T^{\text{miss}}$  (left) and  $p_T(\mu)$  (right) distributions in the W-CR for the Tau-Muon channel. The same sign data and MC events are scaled with  $r_{\text{QCD}}$  before the latter are subtracted from the corresponding opposite sign MC events. The  $W$ +jets background is additionally scaled with  $k_W^{\text{OS/SS}}$ . The hatched bands represent the statistical error of the SM expectation. The lower panels show the ratio between data and SM expectation.

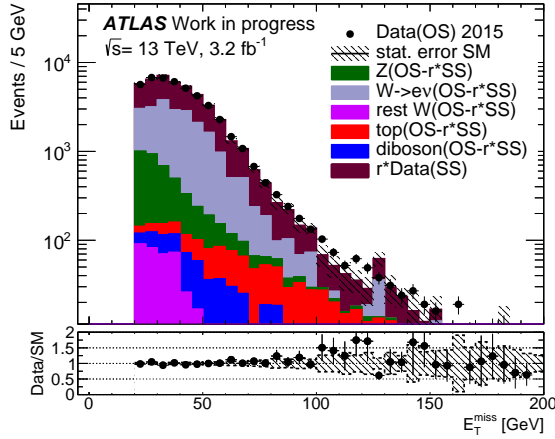
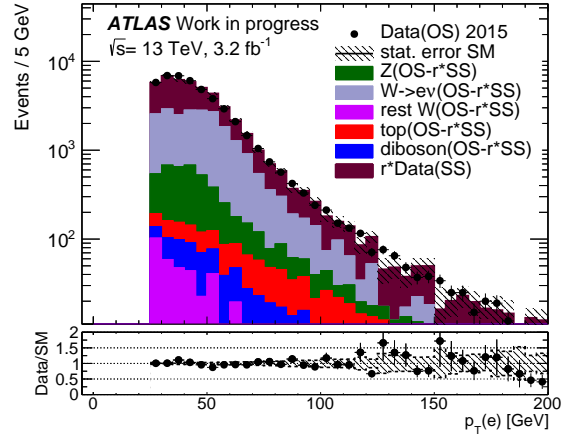
(a) W-CR( $\tau e$ ):  $E_T^{\text{miss}}$ (b) W-CR( $\tau e$ ):  $p_T(e)$ 

Figure 7.8: The measured  $E_T^{\text{miss}}$  (left) and  $p_T(e)$  (right) distributions in the W-CR for the Tau-Electron channel. The same sign data and MC events are scaled with  $r_{\text{QCD}}$  before the latter are subtracted from the corresponding opposite sign MC events. The  $W$ +jets background is additionally scaled with  $k_W^{\text{OS/SS}}$ . The hatched bands represent the statistical error of the SM expectation. The lower panels show the ratio between data and SM expectation.



Sample	Tau-Muon selection:	Tau-Electron selection:
$Z \rightarrow ee$ : OS-rSS	$0 \pm 0$	$1860 \pm 40$
$Z \rightarrow \mu\mu$ : OS-rSS	$0 \pm 35$	$0 \pm 0$
$Z \rightarrow \tau\tau$ : OS-rSS	$1641 \pm 28$	$1344 \pm 24$
$W \rightarrow e\nu$ : OS-rSS	$0 \pm 0$	$17800 \pm 600$
$W \rightarrow \mu\nu$ : OS-rSS	$11600 \pm 700$	$2 \pm 5$
$W \rightarrow \tau\nu$ : OS-rSS	$200 \pm 60$	$360 \pm 60$
$t\bar{t}$ : OS-rSS	$430 \pm 10$	$585 \pm 11$
single top: OS-rSS	$96.5 \pm 3.3$	$141.9 \pm 3.2$
Diboson: OS-rSS	$407 \pm 6$	$493 \pm 6$
r*Data(SS)	$27690 \pm 330$	$22730 \pm 200$
total SM:	$42100 \pm 800$	$45300 \pm 700$
Data(OS):	41892	45270

Table 7.9: Event yields in the W-CR for the Tau-Muon and Tau-Electron selection after subtracting the with  $r_{\text{QCD}}$  scaled SS events from the OS events. The  $W$ +jets backgrounds are also scaled with  $k_{\text{W}}^{\text{OS/SS}}$ . The uncertainties represent the statistical errors.

fluctuations a good agreement between data and SM expectation is observed. Since the multi-jet contribution is included the discrepancy at low  $E_{\text{T}}^{\text{miss}}$  in the Tau-Electron channel, visible in Section 7.6, now vanishes.

## 7.7 Z Control Region

For the Z control region mainly events from the  $Z(\rightarrow \tau\tau)$ +jets contribution should be selected where for the Tau-Muon/Tau-Electron channel one tau decays further into a muon/electron (and two neutrinos) and the other tau decays hadronically. Therefore in this region a real light lepton and a real tau is selected. This can be used to check the real tau modeling in the  $Z$ +jets MC samples and to measure the efficiencies of the single tau triggers (see Section 8.1).

But there are also other SM processes which contribute in this region after all the selection cuts are applied. How and why this is the case is discussed shortly for both regions.

In the Tau-Muon channel the largest contributions are from  $W(\rightarrow \mu\nu)$ +jets and QCD multi-jet events. In the former the muon is correctly identified while the selected tau is a fake tau wrongly reconstructed from a jet. In the latter the muon comes from a semi-leptonic decay inside a jet or is misidentified from a jet and the tau is again fake. The  $Z(\rightarrow ee)$ +jets and  $W(\rightarrow e\nu)$ +jets background are negligible for this selection. For the  $Z(\rightarrow \mu\mu)$ +jets either one muon is not identified and a jet fakes a tau or one muon is reconstructed as a tau. In the  $W(\rightarrow \tau\nu)$ +jets process the tau from the  $W$  boson decays

further into a muon while the selected tau again comes from a wrongly reconstructed jet. For the top background the muon can come from the leptonic decay of the  $W$  boson ( $t \rightarrow Wb$ ) while the tau is either a fake tau misidentified from a jet or a real tau if there is a second leptonically decaying  $W$  boson (for  $t\bar{t}$  or  $Wt$  production). In the case of the diboson background a muon and a tau can be found if one or both vector bosons decay leptonically or when one of them decays hadronically and a jet is then misidentified as a tau.

In contrast to the Tau-Muon selection the Tau-Electron selection has more contribution from other processes. This is mainly the case because it is more probable for an electron to be wrongly reconstructed from a jet than for a muon and also because an electron can be more easily misidentified as a tau. So the largest backgrounds in the Tau-Electron channel are the  $W(\rightarrow e\nu)$ +jets containing a real electron and a fake tau, QCD multi-jet consisting of fake tau and an electron (either from a semi-leptonic decay in a jet or a jet mis-reconstructed as an electron) and  $Z(\rightarrow ee)$ +jets where one electron was wrongly reconstructed as a tau and the second electron identified correctly. The  $Z(\rightarrow \mu\mu)$ +jets and  $W(\rightarrow \mu\nu)$ +jets are negligible and the rest, i.e.  $W(\rightarrow \tau\nu)$ +jets, top and diboson, have similar contribution as in the Tau-Muon channel.

Again the preselection defined in Section 7.3 must be fulfilled for the respective channel and the light lepton also needs to be a signal lepton (cf. Section 5.1) to suppress the multi-jet background. To further reject this background the selected tau is required to have a transverse momentum larger than 25 GeV. To discriminate against the  $W$ +jets background the transverse mass of the light lepton and the  $E_T^{\text{miss}}$  must be smaller than 50 GeV. To reduce the  $W$ +jets background further (and to some extent also the multi-jet background) the condition  $\sum_{i=\mu/e,\tau} \cos(\Delta\phi(i, E_T^{\text{miss}})) > -0.5$  must be fulfilled which is defined as:

$$\sum_{i=\mu/e,\tau} \cos(\Delta\phi(i, E_T^{\text{miss}})) = \cos(\Delta\phi(\mu/e, E_T^{\text{miss}})) + \cos(\Delta\phi(\tau, E_T^{\text{miss}}))$$

For the  $Z(\rightarrow \tau\tau)$ +jets contribution the direction of the  $E_T^{\text{miss}}$  is in general between the two tau decay products (i.e. between the hadronically decaying tau and the light lepton). This leads to a rather small angle  $\phi$  between the tau/light lepton and the  $E_T^{\text{miss}}$ , therefore the sum of the cosines is mostly larger than -0.5. In contrast to that for the  $W$ +jets background the  $E_T^{\text{miss}}$  direction corresponds to the direction of the neutrino from the  $W$  boson decay. The  $\Delta\phi$  of the  $E_T^{\text{miss}}$  and the light lepton is in general quite large, leading to a negative value of the cosine while the angle between the  $E_T^{\text{miss}}$  and the fake tau shows a more even distribution. This lead to quite a lot of  $W$ +jets events where the sum of the cosines is smaller than -0.5 and it can be used to discriminate against  $W$ +jets events. Since for the multi-jet background the  $\sum_{i=\mu/e,\tau} \cos(\Delta\phi(i, E_T^{\text{miss}}))$  shows an even distribution, cutting on this variable will also reduce the multi-jet background to some extent. To suppress the top background again a  $b$ -jet veto is used. To further enhance the  $Z(\rightarrow \tau\tau)$ +jets contribution the invariant mass of the selected tau and the selected light lepton must be between 45 GeV and 85 GeV. The reason why the interval is not around

90 GeV (the  $Z$  boson mass) is that the neutrinos are not considered for the calculation of the invariant mass. The selection cuts for the Z-CR are summarized in Table 7.10.

Tau-Muon Z-CR selection:	Tau-Electron Z-CR selection:
Tau-Muon preselection muon is signal muon $p_T(\tau) > 25 \text{ GeV}$ $m_T(\mu, E_T^{\text{miss}}) < 50 \text{ GeV}$ $\sum_{i=\mu,\tau} \cos(\Delta\phi(i, E_T^{\text{miss}})) > -0.5$ $b$ -jet veto $45 \text{ GeV} < m_{\text{inv}}(\tau, \mu) < 85 \text{ GeV}$	Tau-Electron preselection electron is signal electron $p_T(\tau) > 25 \text{ GeV}$ $m_T(e, E_T^{\text{miss}}) < 50 \text{ GeV}$ $\sum_{i=e,\tau} \cos(\Delta\phi(i, E_T^{\text{miss}})) > -0.5$ $b$ -jet veto $45 \text{ GeV} < m_{\text{inv}}(\tau, e) < 85 \text{ GeV}$

Table 7.10: Definition of the Tau-Muon Z control region and Tau-Electron Z control region.

The number of events in the OS and SS region passing the selection for the Z-CR are given in Table 7.11 for the Tau-Muon and the Tau-Electron channel. The  $W$ +jets backgrounds are scaled with the respective  $k_W^{\text{OS/SS}}$  factor. As one can see from the table about the same number of  $Z(\rightarrow \tau\tau)$ +jets are selected in both channels. This leads to a purity of the selection for the Tau-Muon of about 72 % and for the Tau-Electron channel of roughly 49 %. The lower purity in the latter is mainly due to the high contributions from  $Z(\rightarrow ee)$ +jets and multi-jet background. The purity of the Tau-Electron selection could be increased by using additional cuts, but this also would reduce the statistic quite a lot.

Sample:	Tau-Muon selection:		Tau-Electron selection:	
	OS	SS	OS	SS
$Z \rightarrow ee$ :	0±0	0±0	1651±26	343±12
$Z \rightarrow \mu\mu$ :	176±8	99±6	0±0	0±0
$Z \rightarrow \tau\tau$ :	9850±60	96±6	9790±60	136±7
$W \rightarrow e\nu$ :	0±0	0±0	1380±60	550±40
$W \rightarrow \mu\nu$ :	1240±60	590±40	0±0	0±0
$W \rightarrow \tau\nu$ :	201±20	51±11	240±23	58±12
$t\bar{t}$ :	59.7±2.4	16.7±1.3	64.2±2.6	19.7±1.4
single top:	12.2±0.6	4.7±0.4	15.8±0.7	5.2±0.4
Diboson:	58.5±1.9	7.6±0.7	67.1±2.1	9.8±0.9
total MC:	11600±90	860±40	13210±90	1130±40
data:	13617	2396	20101	6913

Table 7.11: MC and data event yields in the Z-CR for the Tau-Muon and Tau-Electron selection in the opposite sign and the same sign region. The  $W$ +jets backgrounds are scaled with  $k_W^{\text{OS/SS}}$ . The uncertainties represent the statistical errors.

The event yields for the Z control region are shown in Table 7.12. The same sign events

in data and MC are scaled with  $r_{\text{QCD}}$  and the MC events are then subtracted from the corresponding opposite sign MC events. In the Tau-Muon selection the SM expectation is a bit higher than the selected data events whereas in the Tau-Electron selection contains more data events than events from the SM expectation. Nevertheless in the kinematic distributions a good agreement between data and SM expectation can be observed within statistical fluctuations. The distributions of the  $E_{\text{T}}^{\text{miss}}$ ,  $p_{\text{T}}(\mu/e)$ ,  $p_{\text{T}}(\tau)$  and the invariant mass of the tau and the light lepton is shown in Figure 7.9 for the Tau-Muon channel and in Figure 7.10 for the Tau-Electron channel.

Sample	Tau-Muon selection:	Tau-Electron selection:
$Z \rightarrow ee$ : OS-rSS	$0 \pm 0$	$1278 \pm 29$
$Z \rightarrow \mu\mu$ : OS-rSS	$31 \pm 13$	$0 \pm 0$
$Z \rightarrow \tau\tau$ : OS-rSS	$9710 \pm 70$	$9640 \pm 60$
$W \rightarrow e\nu$ : OS-rSS	$0 \pm 0$	$780 \pm 70$
$W \rightarrow \mu\nu$ : OS-rSS	$380 \pm 80$	$0 \pm 0$
$W \rightarrow \tau\nu$ : OS-rSS	$127 \pm 25$	$177 \pm 27$
$t\bar{t}$ : OS-rSS	$35.4 \pm 3$	$42.8 \pm 3$
single top: OS-rSS	$5.4 \pm 0.8$	$10.1 \pm 0.8$
Diboson: OS-rSS	$47.4 \pm 2.1$	$56.4 \pm 2.3$
r*Data(SS)	$3490 \pm 80$	$7528 \pm 100$
total SM:	$13830 \pm 140$	$19520 \pm 140$
Data(OS):	13617	20101

Table 7.12: Event yields in the Z-CR for the Tau-Muon and Tau-Electron selection after subtracting the with  $r_{\text{QCD}}$  scaled SS events from the OS events. The  $W$ +jets backgrounds are also scaled with  $k_{\text{W}}^{\text{OS/SS}}$ . The uncertainties represent the statistical errors.

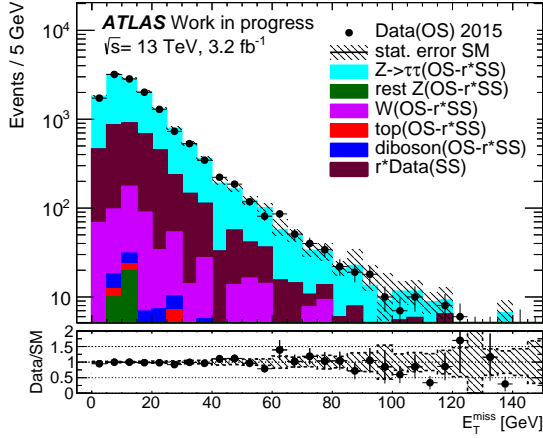
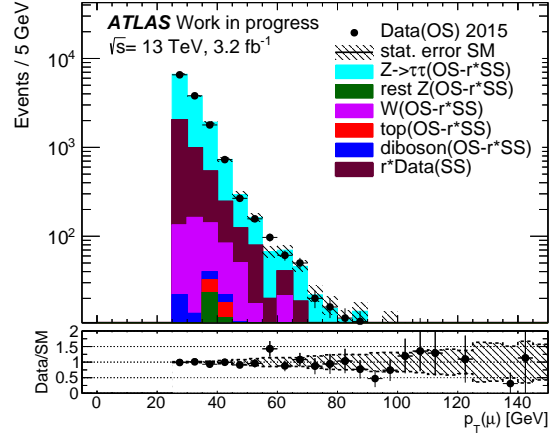
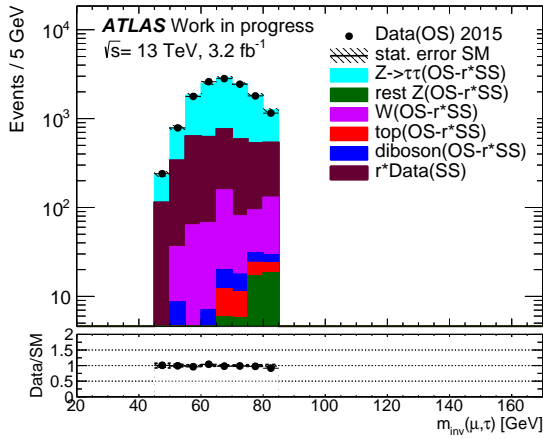
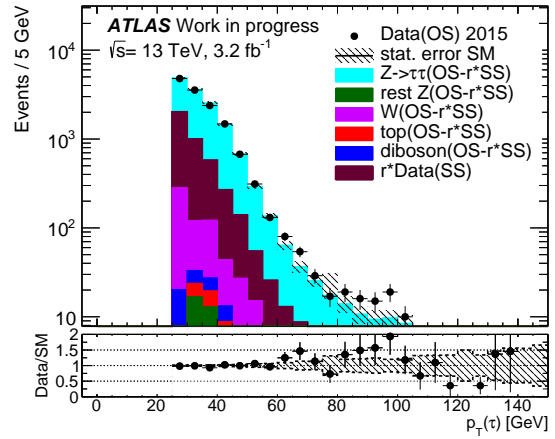
(a) Z-CR( $\tau\mu$ ):  $E_T^{\text{miss}}$ (b) Z-CR( $\tau\mu$ ):  $p_T(\mu)$ (c) Z-CR( $\tau\mu$ ):  $m_{\text{inv}}(\tau, \mu)$ (d) Z-CR( $\tau\mu$ ):  $p_T(\tau)$ 

Figure 7.9: The measured  $E_T^{\text{miss}}$  (top left),  $p_T(\mu)$  (top right),  $m_{\text{inv}}(\mu, \tau)$  (bottom left) and  $p_T(\tau)$  (bottom right) distributions in the Z-CR for the Tau-Muon channel. The same sign data and MC events are scaled with  $r_{\text{QCD}}$  before the latter are subtracted from the corresponding opposite sign MC events. The  $W$ +jets background is additionally scaled with  $k_W^{\text{OS/SS}}$ . The hatched bands represent the statistical error of the SM expectation. The lower panels show the ratio between data and SM expectation.

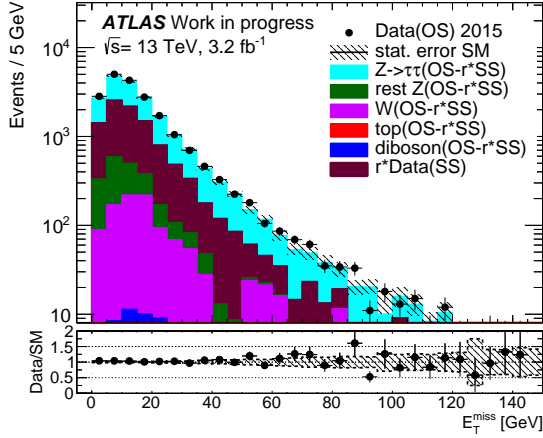
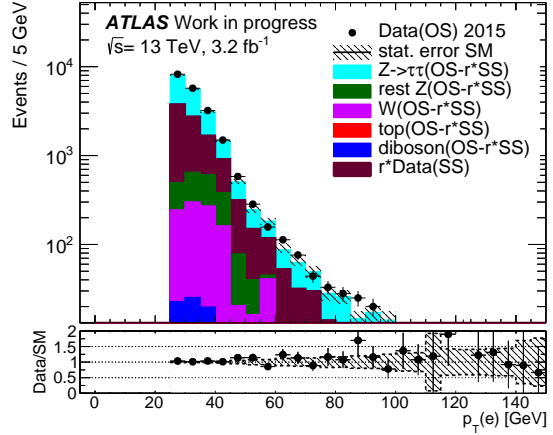
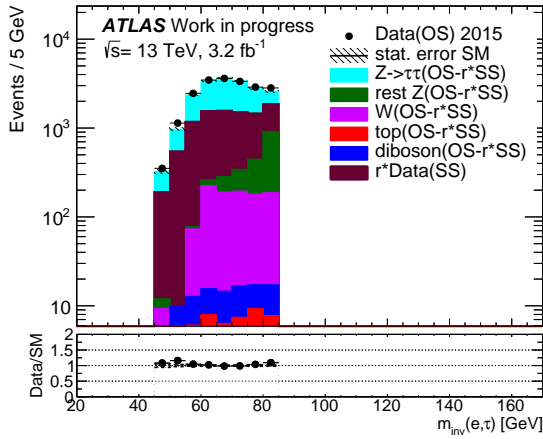
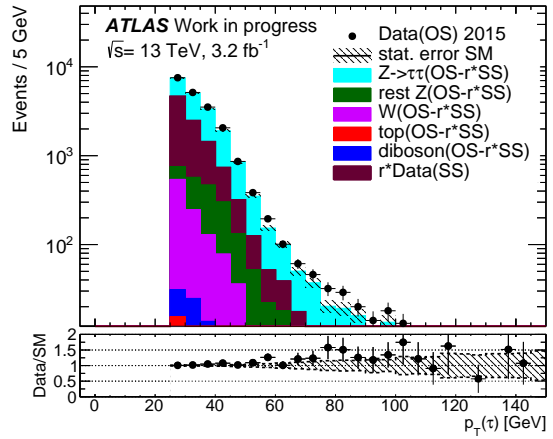
(a) Z-CR( $\tau e$ ):  $E_T^{\text{miss}}$ (b) Z-CR( $\tau e$ ):  $p_T(e)$ (c) Z-CR( $\tau e$ ):  $m_{\text{inv}}(e, \tau)$ (d) Z-CR( $\tau e$ ):  $p_T(\tau)$ 

Figure 7.10: The measured  $E_T^{\text{miss}}$  (top left),  $p_T(e)$  (top right),  $m_{\text{inv}}(e, \tau)$  (bottom left) and  $p_T(\tau)$  (bottom right) distributions in the Z-CR for the Tau-Electron channel. The same sign data and MC events are scaled with  $r_{\text{QCD}}$  before the latter are subtracted from the corresponding opposite sign MC events. The  $W$ +jets background is additionally scaled with  $k_W^{\text{OS/SS}}$ . The hatched bands represent the statistical error of the SM expectation. The lower panels show the ratio between data and SM expectation.

# Chapter 8

## Results: Efficiency of the Di-Tau Trigger

In this section the results of the efficiency measurement of the tau triggers are presented. In Section 8.1 the efficiency of the single tau triggers are measured in data and compared to the efficiency using the events from the MC  $Z(\rightarrow \tau\tau)+\text{jets}$  process and from MC signal samples. In addition the offline  $p_T$  threshold to be in the plateau region of the trigger (see Section 6.2) of the single tau triggers is determined. In Section 8.2 the result of the closure test is shown and the efficiency of the di-tau trigger in data and MC is given.

### 8.1 Efficiency of Single Tau Triggers

The trigger efficiency of single tau triggers, Tau25 and Tau35, is measured in data. These triggers select events which contain at least one hadronically decaying tau with minimal online transverse momentum of 25 GeV and 35 GeV respectively (see Section 6.1). For the efficiency measurement only real taus should be used. To achieve this the Z-CR is utilized where most of the events comes from the  $Z(\rightarrow \tau\tau \rightarrow \tau_{\text{had}}\tau_{\mu/e})$  process for the Tau-Muon/Tau-Electron channel and therefore fulfill the condition of real taus. Nevertheless the contributions from other background processes have to be taken into account. For that the trigger efficiency in data  $\epsilon_{\text{data}}$  is determined by subtracting these other background events from the data events:

$$\epsilon_{\text{data}} = \frac{N_{\text{triggered}}(\text{data}) - N_{\text{triggered}}(\text{otherSM})}{N_{\text{total}}(\text{data}) - N_{\text{total}}(\text{otherSM})}$$

$N_{\text{total}}$  are all selected events from the Z control region and  $N_{\text{triggered}}$  are all these events where additionally the selected tau has fired the corresponding single tau trigger, i.e. it must be matched to an online tau which fulfill the selection criteria of the trigger. The ‘otherSM’ consists of the  $Z(\rightarrow \mu\mu/ee)+\text{jets}$ , the  $W+\text{jets}$ , the top, the diboson and the multi-jet backgrounds.

In the Z-CR the single tau trigger efficiencies using the events from the MC  $Z(\rightarrow \tau\tau)+\text{jets}$  process are also determined. This is done to compare the results and to check that the modeling of the trigger decision in the MC simulation is in agreement with data. The efficiency is calculated using:

$$\epsilon_{\text{MC}(Z(\rightarrow\tau\tau)+\text{jets})} = \frac{N_{\text{triggered}}(\text{MC}(Z(\rightarrow\tau\tau)+\text{jets}))}{N_{\text{total}}(\text{MC}(Z(\rightarrow\tau\tau)+\text{jets}))}$$

$N_{\text{total}}$  here are all events from the  $Z(\rightarrow\tau\tau)+\text{jets}$  process in the Z-CR and  $N_{\text{triggered}}$  are all the events which in addition fulfill the online requirements of the corresponding single tau trigger and where the offline tau is matched to the online tau.

The single tau trigger efficiency is also determined for events from the MC signal samples which are used in Section 8.2 for the closure test. For the measurement events are selected which must contain at least one tau with transverse momentum larger than 25 GeV and pass the event quality requirements defined in Section 5.3. This selection is the same for the Tau-Muon and Tau-Electron channel. In addition in the numerator of the efficiency calculation the selected tau must have fired the corresponding single tau trigger.

$$\epsilon_{\text{MC}(\text{signal samples})} = \frac{N_{\text{triggered}}(\text{MC}(\text{signal samples}))}{N_{\text{total}}(\text{MC}(\text{signal samples}))}$$

In the MC  $Z(\rightarrow\tau\tau)+\text{jets}$  and MC signal samples it was checked that nearly all of the selected taus are indeed real taus, using the truth variables available in MC simulations. Therefore an additional requirement for the selected tau in the MC samples to be a true tau was not used for the efficiency measurement.

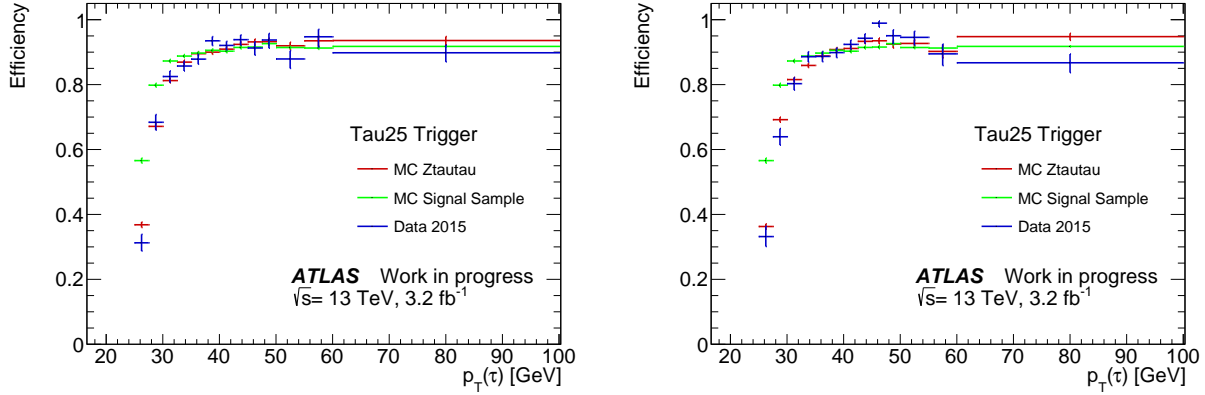
In Figure 8.1 the efficiency for all three cases discussed above is plotted against the transverse momentum of the selected offline tau for the Tau25 trigger in the Tau-Muon channel (left) and in the Tau-Electron channel (right). From these plots the offline threshold for the Tau25 trigger is determined to be 40 GeV, which means that the transverse momentum of the selected offline tau must be larger than 40 GeV to be in the plateau region of the trigger. The same is done for the Tau35 trigger in Figure 8.2 and the offline threshold is 50 GeV. The online and offline thresholds of the single tau triggers are summarized in Table 8.1.

single tau trigger	HLT online threshold	offline threshold
Tau25	25 GeV	40 GeV
Tau35	35 GeV	50 GeV

Table 8.1: Online and offline threshold of the two considered single tau triggers Tau25 and Tau35.

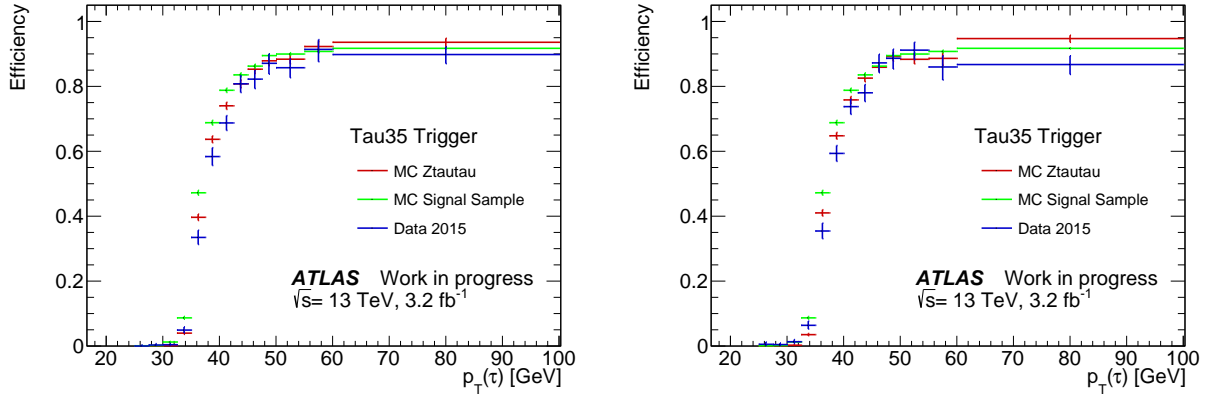
In the Tau-Muon channel a good agreement between all three plotted efficiencies is seen in the plateau region for both triggers. Below the offline thresholds there are some discrepancies especially between data and MC signal samples but this should be of no





(a) Z-CR( $\tau\mu$ ): Turn-on curve of Tau25 trigger (b) Z-CR( $\tau e$ ): Turn-on curve of Tau25 trigger

Figure 8.1: Efficiency of the single tau trigger Tau25 for data, for MC  $Z(\tau\tau)$ +jets events and for the events from MC signal samples for both the Tau-Muon channel (left) and the Tau-Electron channel (right) plotted against the transverse momentum of the selected tau. The offline threshold of this trigger is determined to be 40 GeV from the plots.



(a) Z-CR( $\tau\mu$ ): Turn-on curve of Tau35 trigger (b) Z-CR( $\tau e$ ): Turn-on curve of Tau35 trigger

Figure 8.2: Efficiency of the single tau trigger Tau35 for data, for MC  $Z(\tau\tau)$ +jets events and for events from MC signal samples for both the Tau-Muon channel (left) and the Tau-Electron channel (right) plotted against the transverse momentum of the selected tau. The offline threshold of this trigger is determined to be 50 GeV from the plots.

consequence because in general for an analysis the selection is chosen in such a way that the trigger is fully efficient, i.e. only events in the plateau region of the trigger are selected.

In the Tau-Electron channel there are also some discrepancies in the plateau region of both trigger which are mainly because of the lower purity in the Z-CR for this channel. This leads to fluctuations in the data efficiency due to the subtraction of the other background processes.

## 8.2 Efficiency of the Di-Tau Trigger

The di-tau trigger selects events containing at least two hadronically decaying taus with a minimal online transverse momentum of 35 GeV for one tau and 25 GeV for the other tau (6.1). This trigger is too complex to measure its efficiency directly in data, but it can be determined from MC simulation. Therefore a closure test with MC signal samples is done to prove that the two components of the di-tau trigger are not correlated and its efficiency in data can be calculated as the product of the two corresponding single tau trigger efficiencies (see Section 6.4).

The MC signal samples are used in order to have enough statistic to get a good result for the di-tau trigger efficiency. The list of the MC signal samples is given in Table A.1. The event selection for the efficiency measurement must fulfill the quality requirements described in Section 5.3 and an event must contain at least two taus with a transverse momentum of the leading tau bigger than 50 GeV and of the sub-leading tau larger than 40 GeV. This ensures that the efficiency is only measured in the plateau region of the two corresponding single tau triggers and therefore also in the plateau region of the di-tau trigger.

The efficiency of the di-tau trigger is calculated using the number of selected events in the denominator and the number of events which in addition have fired the di-tau trigger and where both offline taus are matched to two different online taus for the numerator.

$$\epsilon_{\text{MC}(\text{signal samples})} = \frac{N_{\text{triggered}}(\text{MC signal samples})}{N_{\text{total}}(\text{MC signal samples})}$$

The efficiencies of the single tau triggers are calculated analogously where instead of the di-tau trigger the corresponding single tau trigger must have fired and one of the offline taus is matched to an online tau. The efficiencies of the di-tau trigger and the two corresponding single tau triggers are plotted against the transverse momentum of the leading and the sub-leading tau in Figure 8.3.

From the resulting efficiencies the closure of the di-tau trigger can be calculated with Equation 6.1 and 6.2. The efficiencies of the di-tau trigger and of the two single tau triggers as well as the product of the single trigger efficiencies and the closure are given in Table 8.2. The deviation of the closure from one is less than 0.5 %, therefore the two components of the di-tau trigger are not correlated with each other and its efficiency in data can be calculated as the product of the two single tau trigger efficiencies.

The efficiencies of the single tau triggers and the calculated di-tau trigger efficiency in data and for events from the  $Z(\rightarrow \tau\tau)+\text{jets}$  process are given in Table 8.3 for the Tau-Muon and the Tau-Electron selection. Within the statistical errors a good agreement between MC simulation and data in both channels is observed for the single tau trigger efficiencies as well as for the calculated di-tau trigger efficiency. The trigger decision in MC simulation is well modeled in the plateau region of the tau triggers.

For the single tau triggers the efficiencies in the plateau region is measured to be around 90 % and for the di-tau trigger it is higher than 80 %.

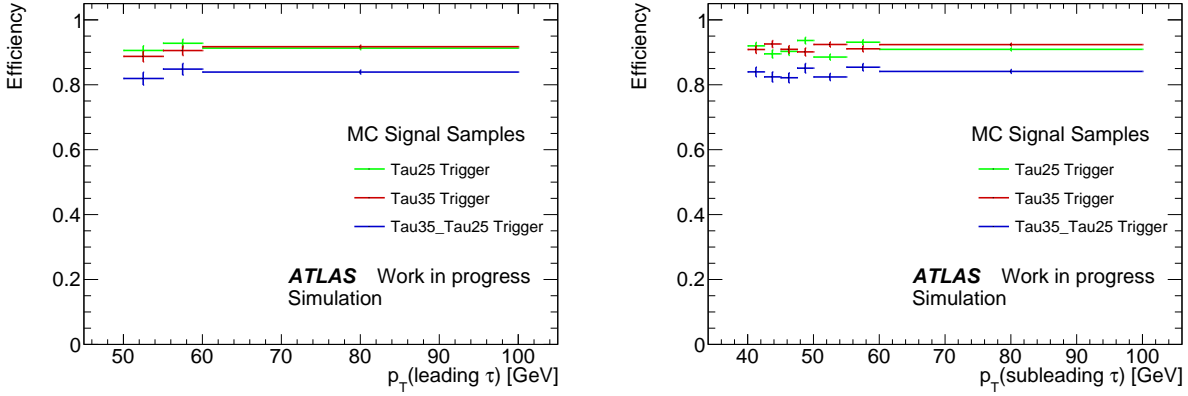


Figure 8.3: Efficiencies of the di-tau trigger and the two corresponding single tau triggers plotted against the transverse momentum of the leading tau (left) and the sub-leading tau (right) using MC signal samples.

	Efficiency:
$\epsilon(\text{Tau25})$ (MC signal samples)	$0.911 \pm 0.013$
$\epsilon(\text{Tau35})$ (MC signal samples)	$0.921 \pm 0.013$
$\epsilon(\text{di-tau})$ (MC signal samples)	$0.841 \pm 0.012$
$\epsilon(\text{Tau25}) \cdot \epsilon(\text{Tau35})$ (MC signal samples)	$0.839 \pm 0.016$
<b>Closure:</b>	<b><math>1.003 \pm 0.024</math></b>

Table 8.2: Efficiencies of the di-tau trigger, the corresponding two single tau triggers and the product of their efficiencies using MC signal samples. For the di-tau trigger also the resulting closure is given. The uncertainties represent the statistical errors.

Efficiency	Tau-Muon channel	Tau-Electron channel
$\epsilon(\text{Tau25})$ (MC $Z(\rightarrow \tau\tau)+\text{jets}$ )	$0.922 \pm 0.018$	$0.924 \pm 0.018$
$\epsilon(\text{Tau35})$ (MC $Z(\rightarrow \tau\tau)+\text{jets}$ )	$0.91 \pm 0.04$	$0.91 \pm 0.04$
$\epsilon(\text{Tau25}) \cdot \epsilon(\text{Tau35})$ (MC $Z(\rightarrow \tau\tau)+\text{jets}$ )	$0.84 \pm 0.04$	$0.84 \pm 0.04$
$\epsilon(\text{Tau25})$ (data)	$0.92 \pm 0.04$	$0.93 \pm 0.04$
$\epsilon(\text{Tau35})$ (data)	$0.88 \pm 0.07$	$0.89 \pm 0.07$
<b><math>\epsilon(\text{Tau25}) \cdot \epsilon(\text{Tau35})</math> (data)</b>	<b><math>0.81 \pm 0.07</math></b>	<b><math>0.83 \pm 0.07</math></b>

Table 8.3: Efficiencies of the single tau triggers measured for events from the  $Z(\rightarrow \tau\tau)+\text{jets}$  process and from data using the Z-CR selection in the Tau-Muon channel and Tau-Electron channel. The di-tau trigger efficiency is calculated as the product of the single tau trigger efficiencies. The uncertainties represent the statistical errors.



# Chapter 9

## Conclusion

In this thesis the measurement of the efficiency of the di-tau trigger, which selects events with at least two hadronically decaying taus with a minimal online transverse momentum for the leading/sub-leading tau of 35 GeV/25 GeV, was presented. The full dataset recorded in 2015 by the ATLAS detector in proton-proton collisions at a center-of-mass energy  $\sqrt{s} = 13$  TeV, corresponding to an integrated luminosity of approximately  $3.2 \text{ fb}^{-1}$ , was used.

The di-tau trigger efficiency was determined in two steps. First the efficiency of the two single tau triggers (Tau25 and Tau35), which correspond to the two components of the di-tau trigger, was measured using a ‘tag-and-probe’ method. Second the efficiency of the di-tau trigger was calculated from the product of the two single tau trigger efficiencies after proving with a closure test that the two components are independent.

For the first step the efficiency in data was compared to the SM expectation. The multi-jet background was estimated from data while all other processes were estimated from MC simulation, where the  $W$ +jets background is additionally normalized to data in a dedicated control region. Two different channels were considered, one where a tau and a muon and one where a tau and an electron were selected. Three different control regions were defined: the  $W$ -CR was used to check the fake tau modeling and to normalize the  $W$ +jets background, the QCD-CR was needed for the multi-jet estimation and in the  $Z$ -CR the real tau modeling was checked and the single tau trigger efficiencies were measured. In all three control regions and in both channels a reasonable agreement between data and SM expectation was found.

The offline threshold of the single tau triggers was determined to be 40 GeV for the Tau25 and 50 GeV for the Tau35 trigger and a good agreement between data and MC in the plateau region was found for the efficiencies. Furthermore the efficiency of both single tau triggers was determined to be around 90 %.

In the second step the independency of the single tau triggers was proven with a closure test using MC samples. The closure test proved that the two components of the di-tau trigger are not correlated. Therefore the di-tau trigger efficiency can be calculated as the product of the two corresponding single tau trigger efficiencies and was determined to be higher than 80 % in the plateau region.



# Appendix A

## MC Background and Signal Samples

Sample:	Name:
392100	MadGraphPythia8EvtGen_A14NNPDF23LO_C1C1_Stau_100p0_0p0
392114	MadGraphPythia8EvtGen_A14NNPDF23LO_C1C1_Stau_182p5_117p5
392126	MadGraphPythia8EvtGen_A14NNPDF23LO_C1C1_Stau_250p0_0p0
392137	MadGraphPythia8EvtGen_A14NNPDF23LO_C1C1_Stau_300p0_0p0
392153	MadGraphPythia8EvtGen_A14NNPDF23LO_C1C1_Stau_362p5_262p5
392172	MadGraphPythia8EvtGen_A14NNPDF23LO_C1C1_Stau_500p0_0p0
392000	MadGraphPythia8EvtGen_A14NNPDF23LO_C1N2_Stau_100p0_0p0
392014	MadGraphPythia8EvtGen_A14NNPDF23LO_C1N2_Stau_182p5_117p5
392026	MadGraphPythia8EvtGen_A14NNPDF23LO_C1N2_Stau_250p0_0p0
392137	MadGraphPythia8EvtGen_A14NNPDF23LO_C1C1_Stau_300p0_0p0
392053	MadGraphPythia8EvtGen_A14NNPDF23LO_C1N2_Stau_362p5_262p5
392072	MadGraphPythia8EvtGen_A14NNPDF23LO_C1N2_Stau_500p0_0p0

Table A.1: List of MC signal samples used for the closure test:

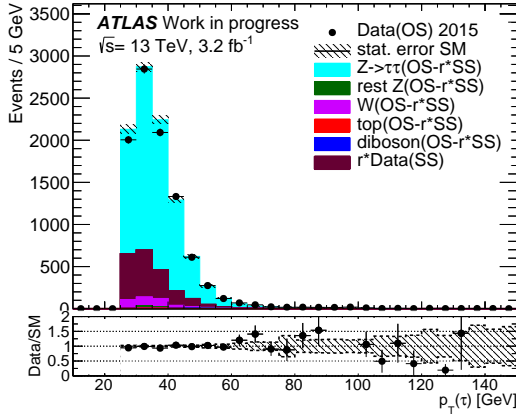
Sample:	Name:	Cross-section [pb]:	k-factor	Filter efficiency:
410000	PowhegPythiaEvtGen_P2012_ttbar_hdamp172p5_nonallhad	831.76	1.	0.543
410007	PowhegPythiaEvtGen_P2012_ttbar_hdamp172p5_allhad	695.99	1.1951	0.4562
410011	PowhegPythiaEvtGen_P2012_singletop_tchan_lept_top	43.739	1.	1.
410012	PowhegPythiaEvtGen_P2012_singletop_tchan_lept_antitop	25.778	1.	1.
410013	PowhegPythiaEvtGen_P2012_Wt_inclusive_top	34.009	1.	1.
410014	PowhegPythiaEvtGen_P2012_Wt_inclusive_antitop	33.989	1.	1.
410015	PowhegPythiaEvtGen_P2012_Wt_dilepton_top	3.5835	1.	1.
410016	PowhegPythiaEvtGen_P2012_Wt_dilepton_antitop	3.5814	1.	1.
361100	PowhegPythia8EvtGen_AZNLOCTEQ6L1_Wplusenu	11306.	1.01724	1.
361101	PowhegPythia8EvtGen_AZNLOCTEQ6L1_Wplusmunu	11306.	1.01724	1.
361102	PowhegPythia8EvtGen_AZNLOCTEQ6L1_Wplustaunu	11306.	1.01724	1.
361103	PowhegPythia8EvtGen_AZNLOCTEQ6L1_Wminusenu	8282.6	1.035786	1.
361104	PowhegPythia8EvtGen_AZNLOCTEQ6L1_Wminusmunu	8282.6	1.035786	1.
361105	PowhegPythia8EvtGen_AZNLOCTEQ6L1_Wminustaunu	8282.6	1.035786	1.
361106	PowhegPythia8EvtGen_AZNLOCTEQ6L1_Zee	1901.2	1.026	1.
361107	PowhegPythia8EvtGen_AZNLOCTEQ6L1_Zmumu	1901.2	1.026	1.
361108	PowhegPythia8EvtGen_AZNLOCTEQ6L1_Ztautau	1901.2	1.026	1.
361063	Sherpa_CT10_llll	12.583	0.91	1.
361064	Sherpa_CT10_lllvSFMinus	1.8446	0.91	1.
361065	Sherpa_CT10_lllvOFMinus	3.6235	0.91	1.
361066	Sherpa_CT10_lllvSFPlus	2.5656	0.91	1.
361067	Sherpa_CT10_lllvOFPlus	5.0169	0.91	1.
361068	Sherpa_CT10_llvv	14.022	0.91	1.
361069	Sherpa_CT10_llvvjj_ss_EW4	0.025765	0.91	1.
361070	Sherpa_CT10_llvvjj_ss_EW6	0.043375	0.91	1.
361081	Sherpa_CT10_WplvWmqq	25.995	0.91	1.
361082	Sherpa_CT10_WpqqWmlv	25.974	0.91	1.
361083	Sherpa_CT10_WlvZqq	12.543	0.91	1.
361084	Sherpa_CT10_WqqZll	3.7583	0.91	1.
361085	Sherpa_CT10_WqqZvv	7.4151	0.91	1.
361086	Sherpa_CT10_ZqqZll	16.59	0.91	0.14253
361087	Sherpa_CT10_ZqqZvv	16.492	0.91	0.28096

Table A.2: List of MC background samples:

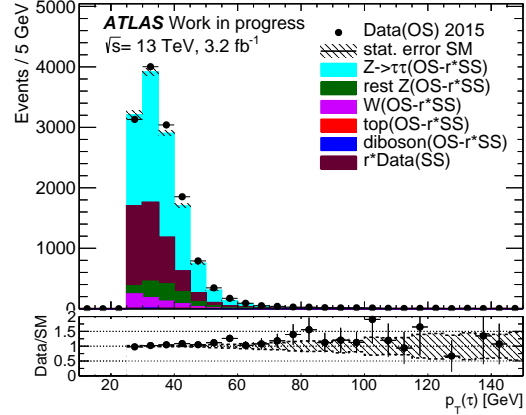


# Appendix B

## Additional Plots



(a) Z-CR( $\tau\mu$ ):  $p_T(\tau)$  after Tau25 trigger



(b) Z-CR( $\tau e$ ):  $p_T(\tau)$  after Tau25 trigger

Figure B.1: The measured  $p_T(\tau)$  distribution after the Tau25 trigger has fired and the offline tau is matched to an online one in the Z-CR for the Tau-Muon channel (left) and the Tau-Electron channel (right). The same sign data and MC events are scaled with  $r_{\text{QCD}}$  before the latter are subtracted from the corresponding opposite sign MC events. The  $W$ +jets background is additionally scaled with  $k_{\text{W}}^{\text{OS/SS}}$ . The hatched bands represent the statistical error of the SM expectation. The lower panels show the ratio between data and SM expectation.

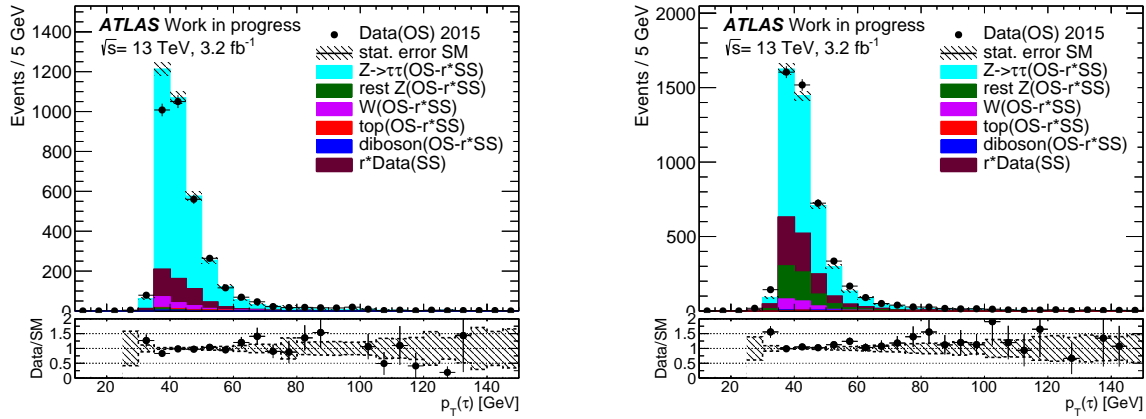
(a) Z-CR( $\tau\mu$ ):  $p_T(\tau)$  after Tau35 trigger(b) Z-CR( $\tau e$ ):  $p_T(\tau)$  after Tau35 trigger

Figure B.2: The measured  $p_T(\tau)$  distribution after the Tau35 trigger has fired and the offline tau is matched to an online one in the Z-CR for the Tau-Muon channel (left) and the Tau-Electron channel (right). The same sign data and MC events are scaled with  $r_{\text{QCD}}$  before the latter are subtracted from the corresponding opposite sign MC events. The  $W$ +jets background is additionally scaled with  $k_W^{\text{OS/SS}}$ . The hatched bands represent the statistical error of the SM expectation. The lower panels show the ratio between data and SM expectation.

# List of Figures

2.1	Evolution of the three inverse coupling constants in the SM (left) and in a supersymmetric extension (right) . . . . .	6
2.2	Diagrams of the considered electroweak production processes . . . . .	11
3.1	CERN Accelerator Complex . . . . .	14
3.2	The ATLAS detector . . . . .	15
3.3	The ATLAS detector functions . . . . .	17
6.1	Example of a turn-on curve . . . . .	32
6.2	Schematic explanation of the tag-and-probe method . . . . .	33
7.1	$E_T^{\text{miss}}$ and $p_T(\mu)$ distributions of the OS events in the W-CR for the Tau-Muon channel . . . . .	42
7.2	$E_T^{\text{miss}}$ and $p_T(e)$ distributions of the OS events in the W-CR for the Tau-Electron channel . . . . .	42
7.3	$E_T^{\text{miss}}$ and $p_T(\mu)$ distributions of the SS events in the W-CR for the Tau-Muon channel . . . . .	43
7.4	$E_T^{\text{miss}}$ and $p_T(e)$ distributions of the SS events in the W-CR for the Tau-Electron channel . . . . .	43
7.5	$E_T^{\text{miss}}$ and $p_T(\mu)$ distributions in the QCD-CR for the Tau-Muon channel . . . . .	46
7.6	$E_T^{\text{miss}}$ and $p_T(e)$ distributions in the QCD-CR for the Tau-Electron channel . . . . .	46
7.7	$E_T^{\text{miss}}$ and $p_T(\mu)$ distributions in the W-CR for the Tau-Muon channel . . . . .	48
7.8	$E_T^{\text{miss}}$ and $p_T(e)$ distributions in the W-CR for the Tau-Electron channel . . . . .	48
7.9	$E_T^{\text{miss}}$ , $p_T(\mu)$ , $m_{\text{inv}}(\mu, \tau)$ and $p_T(\tau)$ distributions in the Z-CR for the Tau-Muon channel . . . . .	53
7.10	$E_T^{\text{miss}}$ , $p_T(e)$ , $m_{\text{inv}}(e, \tau)$ and $p_T(\tau)$ distributions in the Z-CR for the Tau-Electron channel . . . . .	54
8.1	Tau25 trigger efficiency . . . . .	57
8.2	Tau35 trigger efficiency . . . . .	57
8.3	Efficiencies of the di-tau trigger and single tau triggers using MC signal samples . . . . .	59
B.1	$p_T(\tau)$ distribution after Tau25 trigger has fired . . . . .	65

B.2 $p_T(\tau)$ distribution after Tau35 trigger has fired . . . . .	66
--	----

# List of Tables

2.1	The fermions of the SM . . . . .	4
2.2	The bosons of the SM . . . . .	4
2.3	The particle content of the MSSM . . . . .	9
5.1	Selection criteria of physics objects . . . . .	25
7.1	Preselection . . . . .	39
7.2	Definition of W-CR . . . . .	40
7.3	OS and SS event yields in the W-CR . . . . .	41
7.4	The scale factors $k_W^{OS}$ and $k_W^{SS}$ . . . . .	41
7.5	Definition of QCD-CR . . . . .	44
7.6	OS and SS event yields in the QCD-CR . . . . .	45
7.7	The scale factor $r_{QCD}$ . . . . .	45
7.8	Event yields in the QCD-CR . . . . .	47
7.9	Event yields in the W-CR . . . . .	49
7.10	Definition of Z-CR . . . . .	51
7.11	OS and SS event yields in the Z-CR . . . . .	51
7.12	Event yields in the Z-CR . . . . .	52
8.1	Online and offline threshold of the single tau triggers . . . . .	56
8.2	Efficiencies of the di-tau and single tau triggers and the resulting closure for the MC signal samples . . . . .	59
8.3	Efficiencies of the di-tau trigger and the single tau triggers in the Z-CR for the $Z(\rightarrow \tau\tau)+jets$ process and data . . . . .	59
A.1	List of MC signal samples used for the closure test . . . . .	63
A.2	List of MC background samples . . . . .	64



# Bibliography

- [1] D. Schaile. Advanced Particle Physics. lecture notes, LMU München.
- [2] D. Griffith. *Introduction to Elementary Particles*. Wiley-VHC, 2008.
- [3] M. Peskin and D. Schroeder. *An Introduction to Quantum Field Theory*. Westview Press, 1995.
- [4] Particle data group. <http://pdg.lbl.gov/>. Accessed: 01.04.2016.
- [5] D. I. Kazakov. Beyond the Standard Model (In Search of Supersymmetry), 2001. arXiv: 0012288 [hep-ph].
- [6] S. P. Martin. A Supersymmetry Primer, 2016. arXiv: 9709356v7 [hep-ph].
- [7] G. Belanger, F. Boudjema, A. Cottrant, A. Pukhov, and A. Semenov. WMAP constraints on SUGRA models with non-universal gaugino masses and prospects for direct detection. *Nucl. Phys.*, B706:411–454, 2005. arXiv: 0407218 [hep-ph].
- [8] S. F. King, J. P. Roberts, and D. P. Roy. Natural dark matter in SUSY GUTs with non-universal gaugino masses. *JHEP*, 10:106, 2007. arXiv: 0705.4219 [hep-ph].
- [9] J. Alwall, P. Schuster, and N. Toro. Simplified Models for a First Characterization of New Physics at the LHC. *Phys. Rev.*, D79:075020, 2009. arXiv: 0810.3921 [hep-ph].
- [10] D. Alves et al. Simplified Models for LHC New Physics Searches. *J. Phys.*, G39:105005, 2012. arXiv: 1105.2838 [hep-ph].
- [11] ATLAS Collaboration. Search for supersymmetry in events with large missing transverse momentum, jets, and at least one tau lepton in 20 fb<sup>-1</sup> of  $\sqrt{s} = 8$  TeV proton-proton collision data with the ATLAS detector. *JHEP*, 103, 2014. arXiv: 1407.0603 [hep-ph].
- [12] ATLAS Collaboration. Search for direct top squark pair production in final states with two tau leptons in pp collisions at  $\sqrt{s} = 8$  TeV with the ATLAS detector. *Eur. Phys. J.*, C76(81), 2016. arXiv: 1509.04976 [hep-ph].
- [13] <http://bigscience.web.cern.ch/bigscience/en/lhc/lhc2.html>. Accessed: 2016-03-07.

- 
- [14] CERN Brochure, LHC the guide. <https://cds.cern.ch/record/1165534/files/CERN-Brochure-2009-003-Eng.pdf>, 2009.
- [15] Cern website:. <http://home.web.cern.ch>. Accessed: 2016-03-08.
- [16] ATLAS Collaboration. The ATLAS Experiment at the CERN Large Hadron Collider. *JINST*, 3:S08003, 2008.
- [17] ATLAS Collaboration. *ATLAS detector and physics performance: Technical Design Report, 1*. Technical Design Report ATLAS. CERN, Geneva, 1999. <https://cds.cern.ch/record/391176>. Accessed: 2016-03-09.
- [18] <http://www.atlas.ch/photos/full-detector-cgi.html>. Accessed: 2016-03-08.
- [19] <http://www.atlas.ch/photos/how-atlas-works.html>. Accessed: 2016-03-10.
- [20] M Cacciari, G. P. Salam, and G. Soyez. The anti- $k_t$  jet clustering algorithm. *JHEP*, 2008(04):064, 2008. arXiv: 0802.1189 [hep-ph].
- [21] ATLAS Collaboration. 2015 start-up trigger menu and initial performance assessment of the ATLAS trigger using Run-2 data. Technical Report ATL-DAQ-PUB-2016-001, CERN, Geneva, Mar 2016. <https://cds.cern.ch/record/2136007>.
- [22] ATLAS Collaboration. The ATLAS Simulation Infrastructure. *Eur. Phys. J.*, C70(3):823–874, 2010.
- [23] S. Alioli, P. Nason, C. Oleari, and E. Re. A general framework for implementing NLO calculations in shower Monte Carlo programs: the POWHEG BOX. *JHEP*, 1006:043, 2010. arXiv: 1002.2581 [hep-ph].
- [24] T. Sjostrand, S. Mrenna, and P. Z. Skands. A Brief Introduction to PYTHIA 8.1. *Comput. Phys. Commun.*, 178:852, 2008. arXiv: 0710.3820 [hep-ph].
- [25] T. Sjostrand, S. Mrenna, and P. Z. Skands. PYTHIA 6.4 Physics and Manual. *JHEP*, 0605:026, 2006. arXiv: hep-ph/0603175 [hep-ph].
- [26] T. Gleisberg, S. Höche, F. Krauss, M. Schönherr, S. Schumann, et al. Event generation with SHERPA 1.1. *JHEP*, 0902:007, 2009. arXiv: 0811.4622 [hep-ph].
- [27] S. Agostinelli et al. GEANT4: A Simulation toolkit. *Nucl. Instrum. Meth.*, A506:250–303, 2003.
- [28] ATLAS Collaboration. Search for direct electro-weakino and slepton production in events with at least two hadronic taus and missing transverse momentum at  $\sqrt{s} = 13$  TeV (supporting INT note). Technical Report ATL-COM-PHYS-2015-1284, CERN, Geneva, Oct 2015. <https://cds.cern.ch/record/2058818>.



- [29] J. Alwall, R. Frederix, S. Frixione, V. Hirschi, F. Maltoni, et al. The automated computation of tree-level and next-to-leading order differential cross sections, and their matching to parton shower simulations. *JHEP*, 1407:079, 2014. arXiv: 1405.0301 [hep-ph].
- [30] ATLAS Collaboration. The simulation principle and performance of the ATLAS fast calorimeter simulation FastCaloSim. Technical Report ATL-PHYS-PUB-2010-013, CERN, Geneva, Oct 2010. <https://cds.cern.ch/record/1300517>.
- [31] ATLAS Collaboration. Jet Calibration and Systematic Uncertainties for Jets Reconstructed in the ATLAS Detector at  $\sqrt{s} = 13$  TeV. Technical Report ATL-PHYS-PUB-2015-015, CERN, Geneva, Jul 2015.
- [32] ATLAS Collaboration. Tagging and suppression of pileup jets with the ATLAS detector. Technical Report ATLAS-CONF-2014-018, CERN, Geneva, May 2014. <https://cds.cern.ch/record/1700870>.
- [33] ATLAS Collaboration. Expected performance of the ATLAS  $b$ -tagging algorithms in Run-2. Technical Report ATL-PHYS-PUB-2015-022, CERN, Geneva, Jul 2015. <https://cds.cern.ch/record/2037697>.
- [34] ATLAS Collaboration. Supporting document on electron identification and efficiency measurements using the 2015 LHC proton-proton collision data. Technical Report ATL-COM-PHYS-2016-041, CERN, Geneva, Jan 2016. <https://cds.cern.ch/record/2125283>.
- [35] ATLAS Collaboration. Muon reconstruction performance in early  $\sqrt{s} = 13$  TeV data. Technical Report ATL-PHYS-PUB-2015-037, CERN, Geneva, Aug 2015. <https://cds.cern.ch/record/2047831>.
- [36] ATLAS Collaboration. Reconstruction, Energy Calibration, and Identification of Hadronically Decaying Tau Leptons in the ATLAS Experiment for Run-2 of the LHC. Technical Report ATL-COM-PHYS-2015-927, CERN, Geneva, Aug 2015. <https://cds.cern.ch/record/2044557>.
- [37] ATLAS Collaboration. Expected performance of missing transverse momentum reconstruction for the ATLAS detector at  $\sqrt{s} = 13$  TeV. Technical Report ATL-PHYS-PUB-2015-023, CERN, Geneva, Jul 2015. <https://cds.cern.ch/record/2037700>.
- [38] ATLAS Collaboration. Selection of jets produced in 13TeV proton-proton collisions with the ATLAS detector. Technical Report ATLAS-CONF-2015-029, CERN, Geneva, Jul 2015. <https://cds.cern.ch/record/2037702>.
- [39] M. Pickering. The ATLAS Hadronic Tau Trigger: Initial Run-2 Strategy and Performance. Technical Report ATL-DAQ-PROC-2015-042, CERN, Geneva, Oct 2015. <https://cds.cern.ch/record/2058716>.

- [40] R. Bielski. The ATLAS Muon Trigger Performance in Run I and Initial Run II Performance. Technical Report ATL-DAQ-PROC-2015-029, CERN, Geneva, Sep 2015. <https://cds.cern.ch/record/2055529>.
- [41] J. Reichert. The Upgrade and Performance of the ATLAS Electron and Photon Triggers Towards Run 2. Technical Report ATL-DAQ-PROC-2015-037, CERN, Geneva, Oct 2015. <https://cds.cern.ch/record/2058100>.
- [42] ATLAS Collaboration. Search for Standard Model  $H \rightarrow \tau^+\tau^- \rightarrow \ell\tau_h$  with the ATLAS Detector in 8TeV Proton-Proton Collisions. Technical Report ATL-COM-PHYS-2013-1494, CERN, Geneva, Nov 2013. <https://cds.cern.ch/record/1624362>.

# Danksagung

Ich möchte mich bei allen Leute bedanken, die mich bei der Anfertigung dieser Arbeit unterstützt haben:

- Prof. Dorothee Schaile, die mir die Möglichkeit gegeben hat an ihrem Lehrstuhl zu arbeiten und diese Arbeit zu verfassen.
- Dr. Federica Legger für die ausgezeichnete Betreuung und für das Korrektur lesen der Arbeit.
- Frau Grimm-Zeidler für die Hilfe bei allen administrativen Fragen.
- Christopher Bock und Balthasar Schachtner für die Hilfe bei technischen Problemen.
- Michael Holzbock für die angenehme Atmosphäre in unserem Büro.
- Allen Mitgliedern des Lehrstuhls für das gute Arbeitsklima
- Meiner Familie und im besonderen meinen Eltern, die mich während meines Studiums immer unterstützt haben.



# Selbstständigkeitserklärung

Hiermit erkläre ich, die vorliegende Arbeit selbstständig verfasst zu haben und keine anderen als die in der Arbeit angegebenen Quellen und Hilfsmittel benutzt zu haben.

München, den 11. Mai 2016

Ort, Datum

\_\_\_\_\_  
Unterschrift